Chemical evolution of calc-alkaline magmas during the ascent through continental crust: constraints from Methana, Aegean arc

Journal:	*Journal of Petrology*
Manuscript ID	JPET-Aug-19-0113.R1
Manuscript Type:	Original Manuscript
Date Submitted by the Author:	07-Jan-2020
Complete List of Authors:	Schoenhofen, Milena; Friedrich-Alexander-Universitat Erlangen-Nurnberg, Endogene Geodynamics; Macquarie University, Earth and Planetary Sciences Haase, Karsten; Universität Erlangen-Nürnberg, GeoZentrum Nordbayern Beier, Christoph; Universität Erlangen-Nürnberg, GeoZentrum Nordbayern; FIN-00014 University of Helsinki, Department of Geosciences and Geography Woelki, Dominic; Friedrich-Alexander-Universitat Erlangen-Nurnberg, Endogene Geodynamics Regelous, Marcel; Universität Erlangen-Nürnberg, GeoZentrum Nordbayern
Keyword:	Aegean arc, assimilation, magma mixing, fractional crystallisation, stagnation

Chemical evolution of calc-alkaline magmas during the ascent through continental crust: constraints from Methana, Aegean arc

Milena V. Schoenhofen[1, 2]*, Karsten M. Haase[1], Christoph Beier[1,3], Dominic Woelki[1], and Marcel Regelous[1]

[1]GeoZentrum Nordbayern, Friedrich-Alexander Universität Erlangen-Nürnberg (FAU), Schlossgarten 5, 91054 Erlangen, Germany

[2]Department of Earth and Planetary Sciences, Macquarie University, Sydney, NSW 2109, Australia

[3]Department of Geosciences and Geography, PO Box 64, FIN-00014 University of Helsinki, Finland

*Corresponding author: milena.schoenhofen@fau.de, Phone: +49/(0)9131/85- 26071

ABSTRACT

Quaternary calc-alkaline andesitic to dacitic lavas effusively erupted on top of about 30 km thick accreted continental crust at Methana peninsula in the western Aegean arc. We present new data of major and trace element concentrations as well as of Sr-Nd-Pb isotope ratios along with mineral compositions of Methana lavas and their mafic enclaves. The enclaves imply a **parental** basaltic magma and fractional crystallisation processes with relatively little crustal assimilation in the deep part of the Methana magma system. The composition of amphibole in some mafic enclaves and lavas indicates deeper crystallisation at ~25 km depth close to the Moho **compared to t**he evolved lavas **that formed at** <15 km depth. The presence of amphibole and low Ca contents in olivine suggest high water contents of ~4 **wt.-%** in the primitive magmas at Methana. The compositions of andesitic and dacitic lavas reflect fractional crystallisation, assimilation of sedimentary material, and magma mixing in the upper 15 km of the crust. The Methana magmas have fO_2 of FMQ +1 to +2 at temperatures of 1200 to 750°C and the fO_2 does not vary systematically from mafic to felsic **compositions** suggesting that the mantle wedge was oxidized by sediment subduction. Amphibole is an important fractionating phase in the more evolved Methana magmas and causes significant changes in incompatible element ratios. Although xenocrysts and mineral compositions indicate magma mixing, the major and trace element variation implies only limited mixing between dacitic and basaltic melts.

KEY WORDS

Magma evolution, assimilation, fractional crystallisation, magma mixing

INTRODUCTION

Calc-alkaline magmas are abundant on Earth and compose large portions of the continental crust (e.g. Rudnick & Gao, 2003) and typically occur at subduction zones where oceanic lithosphere is subducted below lithosphere with thick continental crust (Gill, 1981). Magmas at subduction zones are commonly mixtures of different sources that may include the subducting slab, mantle wedge, and the crust through which the melts ascend (e.g. Davidson, 1987, McCulloch & Gamble, 1991, Wörner *et al.*, 1992). Sedimentary material subducted into the mantle affects the composition of the mantle, melt compositions, crustal growth and volcanism (e.g. Plank & Langmuir, 1993, White & Patchett, 1984) but sediments are also accreted at subduction zones and potentially contaminate the ascending magmas (e.g. Davidson, 1987, McCulloch *et al.*, 1994). Calc-alkaline andesites may form either as primary melts of hydrous upper mantle (Kelemen, 1995, Kushiro, 1974), or as products of assimilation, mixing, and fractional crystallisation of a basaltic melt within the crust (e.g. Grove *et al.*, 2012). The assimilation processes in the continental crust are believed to occur largely in the lower crust where mafic melts cool, mix and react with crustal wall rocks (Annen *et al.*, 2006, Hildreth & Moorbath, 1988). On the other hand, extensive fractional crystallisation in the middle crust associated with assimilation of crustal material produces dacitic to rhyolitic magmas (e.g. Price *et al.*, 2005). Mixing between felsic and mafic melts may lead to intermediate magmas (Reubi & Blundy, 2009) and the different magma batches erupting at continental subduction volcanoes are usually not related by simple fractional crystallisation processes, i.e. they do not represent a liquid line of descent (Eichelberger *et al.*, 2006). The andesitic to rhyolitic magmas at continental subduction zones frequently erupt explosively because of their high viscosities and volatile contents (Eichelberger, 1995). The main parameters determining whether magmas erupt effusively or explosively appear to be magma viscosity, volatile content and evolution,

magma ascent rate but also regional geology (Cassidy *et al.*, 2018). Thus, the processes resulting in the formation and eruption of calc-alkaline magmas are manifold and complex and it is essential to distinguish between primary mantle-related primitive andesites and those formed from shallow level processes in the Earth's continental crust.

Here, we study the processes affecting the evolution of calc-alkaline magmas during ascent through the crust using andesite and dacite lavas and their mafic enclaves from Methana peninsula in the western Aegean arc. The mineral assemblage of the lavas investigated here is dominated by plagioclase and amphibole that provide evidence for combined assimilation and fractional crystallisation processes at shallow crustal levels. Mineral thermobarometry reveals that pressures of crystallisation are generally less than 0.4 GPa at temperatures of ~750 to 1200°C. The continuous range of amphibole pressures and temperatures implies that the magma crystallised largely in the upper crust. The occurrence of mafic enclaves indicates crystal fractionation in the lower crust with little assimilation whereas the more felsic lavas formed by crystallisation, mixing and assimilation of sediments in the upper crust. The presence of the enclaves implies that the mafic magmas ascended into the shallow felsic magma reservoirs with limited and less efficient mixing.

GEOLOGICAL BACKGROUND

Methana peninsula in the Saronic Gulf lies at the western end of the Aegean Arc (Fig. 1) that formed by the subduction of the Ionian Plate underneath the Aegean microplate with a subduction rate of 3.5 cm/year (McClusky *et al.*, 2000). Subduction has been active since 50 million years with southward-directed arc migration as a result of slab-rollback (Jolivet *et al.*, 2013). The volcanic centres along the 500 km-long Aegean arc have been active since the Pliocene (Francalanci *et al.*, 2005). Seismic data indicate a slab depth of 90 to 100 km beneath Methana and anomalously high Vp/Vs ratios at 80 km depth which may indicate hydrated or

partially molten material (Halpaap *et al.*, 2018). Seismic anisotropy suggests trench-parallel mantle flow in the western part of the Aegean arc (Evangelidis, 2017). The subducting lithosphere of the Ionian Plate is **likely** Triassic (~220-230 Ma) in age (Speranza *et al.*, 2012) and consists of 5 to 8 km thick mafic crust covered by ~6 km thick sediments, half of which are pre-Messinian **in age** (de Voogd *et al.*, 1992, Kokinou *et al.*, 2005). The sediment thickness on the subducting slab is up to 8 km in the western Hellenic Trench. **Approximately** about 20 to 60% of this sediment is accreted whereas the remaining portion is subducted (Clift & Vannucchi, 2004, Kopf *et al.*, 2003) although only basaltic crust is observed in seismic profiles at depths >40 km (Pearce *et al.*, 2012). The continental crust beneath the Saronic Gulf is 25 to 30 km thick which **is** comparable to that in the central part of the Aegean arc (Cossette *et al.*, 2016, Sachpazi *et al.*, 2007). The upper crust consists of Mesozoic to Neogene clastic and carbonate sediments as well as ophiolites (Dietrich *et al.*, 1988, Robertson, 2004). Aegean **a**rc lavas range from tholeiitic and calc-alkaline basalts to rhyolites with enriched incompatible element contents, high Sr and Pb and relatively low Nd isotope ratios reflecting mixing of mantle and crustal components (Francalanci *et al.*, 2005). The lavas of Santorini show a notable change in source composition and magma evolution with the older lavas being calc-alkaline whereas the younger rocks show a more tholeiitic **composition** (Andújar *et al.*, 2015, Bailey *et al.*, 2009, Nicholls, 1971).

Methana Peninsula is largely covered by Quaternary subduction-related calc-alkaline andesitic to dacitic lava domes and flows containing mafic enclaves whereas volcaniclastic rocks are rare (Dietrich *et al.*, 1988, Pe, 1974). Pe-Piper and Piper (2013) subdivided the volcanic rocks of Methana into eight units (Fig. 1) based on the geological map of Dietrich and Gaitanakis (1995). The Quaternary magmatic domes and flows diverge from the central area of the peninsula and are largely elongated in an E-W or NE-SW direction (Pe-Piper & Piper, 2013). Most of the volcanism on Methana is younger than 1.5 Ma but some volcanic outcrops

at the coast have been dated at ~3.5 Ma (Fytikas *et al.*, 1984, Matsuda *et al.*, 1999, Pe-Piper & Piper, 2013). The last volcanic eruption occurred around 220 years BC at Mavi Petra in the north-western part of Methana (Fig. 1). The lava compositions range from basaltic andesites to dacites but all lavas also contain numerous mafic enclaves which are mostly basaltic to basaltic andesitic in composition (Dietrich *et al.*, 1988, Elburg *et al.*, 2014, Elburg *et al.*, 2018, Pe, 1974, Woelki *et al.*, 2018). Olivines with **forsterite (**Fo=100*Mg/(Mg+Fe^{2+})) contents >90 are frequent both in the mafic and in the more silicic rocks implying that primary melts with Mg# (Mg# = 100*Mg/(Mg + Fe^{2+})) ~72 must exist in the mantle wedge beneath Methana (Woelki *et al.*, 2018). These olivine **xenocrysts** have relatively high $\delta^{18}O_{VSMOW}$ (VSMOW = Vienna Standard Mean Ocean Water) compositions of ~6.5‰ implying that the mantle wedge contained significant sediment from the subducting slab (Woelki *et al.*, 2018). Geochemical data of the felsic lavas indicate a strong effect of crustal assimilation compared to the mafic rocks and the tectonic regime at Methana probably had a strong influence on the magma ascent (Elburg *et al.*, 2018, Pe-Piper & Piper, 2013). Thus, Elburg et al. (2018) suggested that much of the chemical and isotopic variation in the lavas is due to mixing and mingling processes between basaltic andesite and felsic melts based on whole rock major element, trace element and isotope data and zircon Hf isotope data. The stagnation and mixing of the mafic and felsic melts in the lower and upper crust is believed to depend on variable tectonic phases where lava domes with enclaves form during compressional phases, and felsic pyroclastics and mafic lavas reflect extensional phases (Elburg *et al.*, 2018).

METHODS

Sampling of most major volcanic units in Methana (Fig. 1) was conducted in 2015 on the basis of the **existing** geological maps (Dietrich & Gaitanakis, 1995, Pe-Piper & Piper, 2013). Samples were selected ensuring a minimum degree of alteration **and weathering**. Samples were labelled

using an International Geological Sample Number (IGSN; Table 1). Sample processing started with cutting unaltered pieces for geochemical analysis and thin section preparation. The whole rock pieces were washed in an ultrasonic bath with deionized water and dried for 12 hours at 60°C. The clean geochemistry pieces were crushed using a hydraulic press and reduced to powder in an agate ball mill. The powder was dried for 12 hours at 104 °C prior to fusion for major element analysis.

Whole-rock analyses

Major elements of 86 whole rocks and enclaves were analysed using a Spectro XEPOS He X-ray fluorescence spectrometer at the GeoZentrum Nordbayern, Friedrich-Alexander Universität Erlangen-Nürnberg, Germany. Further details of the analytical techniques are provided in Freund et al. (2013). Accuracy and precision of the measurements were determined by multiple measurements of the international rock standards BE-N and BR. The accuracy is generally better than ~3% (2σ) except for P_2O_5 which is better than 7.5%. The precision is better than 0.1 and 0.2%**, respectively** (further information available in supplemental Table 1). Trace element analyses of 46 Methana lava and enclave samples were determined at the GeoZentrum Nordbayern on a Thermo Fisher Scientific XSeries 2 Quadrupole Inductively Coupled Plasma Mass Spectrometer (ICP-MS) connected to an Aridus 2 membrane desolvating sample introduction system. Repeated measurements of the international rock standards BHVO-2 give a precision and accuracy better than 1.1% (2σ) and 1.1% (2σ), respectively (further details are in supplementary Table 1).

The Sr, Nd and Pb isotope analyses were performed at the GeoZentrum Nordbayern. Strontium and Nd isotopes were analysed using a Thermo-Fischer Triton thermal ionization mass spectrometer (TIMS) in static mode following the chemical and analytical procedures described previously (Haase *et al.*, 2017). Lead isotope procedures and analytical techniques

using a Thermo-Fisher Neptune multicollector plasma ionisation mass spectrometer in static mode are described in detail by Woelki et al. (2018). Strontium isotope measurements were corrected for mass fractionation assuming $^{88}Sr/^{86}Sr = 0.1194$ where mass 85 was monitored to correct the contribution of ^{87}Rb to ^{87}Sr. Neodymium isotope data were corrected for mass fractionation using $^{146}Nd/^{144}Nd = 0.7219$. Samarium interferences on masses 144, 148, 150 are corrected by measuring ^{147}Sm, but the correction was insignificant for all samples. During the measurements, the SRM987 standard yielded $^{87}Sr/^{86}Sr = 0.710259$, and the Erlangen Nd standard gave $^{143}Nd/^{144}Nd = 0.511540$ (corresponding to a value of 0.511850 for the La Jolla Nd isotope standard; see supplemental Table 1). Lead isotope measurements were corrected by $^{205}Tl/^{203}Tl = 2.3871$ for instrumental mass bias and external normalization was conducted by SRM 981 Pb standard (Todt *et al.*, 1996). Repeated measurements of rock standards give an accuracy and reproducibility better than 100 ppm.

Mineral analyses

Mineral major element concentrations were measured using a JEOL JXA 8200 Superprobe electron microprobe at the GeoZentrum Nordbayern, Erlangen, following methods and using standards used in Beier *et al.* (2018). Plagioclase and amphibole were measured with a 3 µm electron beam diameter at 15 kV acceleration voltage and a beam current of 15 nA. Oxides were measured at 20 kV acceleration voltage and with a 1 µm beam diameter with a current of 20 nA. All measured mineral data are presented in supplementary Table 1.

Trace elements on minerals were measured in five thin sections by laser ablation ICP-MS at the GeoZentrum Nordbayern using a UP193FX laser which is coupled with an Agilent 7500c quadrupole ICP-MS (Schulz *et al.*, 2006). External calibration was conducted by NIST SRM 612 glass with given values by (Pearce *et al.*, 1997). Repeated analyses of the basaltic rock standard BCR2g (n = 4) give an accuracy of <10 % for all elements (except Pb <16 % and

Cu <25 %) and a reproducibility of <6 % for all elements (except for Gd, Tm and Yb < 8 % and Sm, Dy and Er <9%).

RESULTS

Petrography and mineral compositions

The Methana lavas are generally highly porphyritic with up to 60% phenocrysts of plagioclase and amphibole and to a lesser extent olivine, clinopyroxene, orthopyroxene, biotite, magnetite, ilmenite, and apatite (Table 2). The lavas typically have <10% vesicles and commonly contain mafic enclaves that differ from their host rocks in petrography and composition. The enclaves are generally fine-grained with a lower proportion of phenocrysts compared to the commonly coarser host lavas. The enclaves consist of plagioclase, amphibole, clinopyroxene, Fe-Ti oxides, and sometimes olivine (Table 2).

Plagioclase is the most abundant mineral in lavas and in most enclaves. Based on their texture and anorthite (An = 100*(Ca/Ca+K+Na)) contents we defined four different generations of plagioclase crystals in the Methana lavas: (1) normally zoned plagioclases with cores of An_{85-77} and rims of An_{44-33} (Fig. 2a); (2) reversely zoned crystals with cores of An_{53-48} and step-like increasing rims to An_{80-68} (Fig. 2b); (3) reversely zoned plagioclase crystals with cores of An_{54-41} and continuously increasing An contents towards the rim reaching An_{70} (Fig. 2c); and (4) sieve-textured plagioclase crystals with oscillatory zoning **and** maximum An contents of 88 and rims with An_{77-46} (Fig. 2d). The enclaves contain two different types of plagioclase phenocrysts; (1) sieve-textured crystals **that have** cores with An contents of 77-44, and (2) plagioclase with rounded and embayed crystals that either display An_{51-44} from core to rim or that display elevated An contents of 93-68. The plagioclase crystals in the mafic enclaves with 6 to 7 wt.-% MgO have high An (70-93) and FeO (>0.4 wt.-%) contents **(Fig. 5d)** whereas

plagioclase in the lavas shows a large range of plagioclase compositions ($An_{33–89}$). The variation of the An contents in plagioclase in all samples is between 40 and 90 (Fig. 3a) **but 59% of the analysed plagioclase compositions (n=776) are between 40 and 50% An (Fig. 3b).**

Amphibole (typically hornblende) is abundant in the Methana enclaves and lavas with Mg# ranging between 77 and 47 **(Fig. 3c).** The Methana lavas contain three different types of amphiboles which can be distinguished based on their shape and composition: (1) Euhedral and normally zoned amphiboles (Fig. 4a) have high Al_2O_3 contents in the cores (10.6 to 12.6 wt.-%) while the rims range from 9.8 to 12.3 wt.-%. Magnesium **numbers (Mg#)** range from 58 to 73 in the rims and from 65 to 72 in the cores. (2) Oscillatory zoned amphiboles (Fig. 4b) display Al_2O_3 contents of up to 14.4 wt.-%. (3) Subhedral to anhedral amphibole have lower Al_2O_3 contents of 7.4 to 9.2 wt.-% in the cores and Al_2O_3 contents from 6.6 to 9.9 wt.-% in the rims. The Mg# of these amphiboles range from 50 to 66 in the rims and 59 to 70 in the cores, i.e. the cores are generally more Mg-rich. The mafic enclaves ME1549 and ME1515 with 6 to 7 wt.-% MgO contain amphiboles that have the highest Al_2O_3 contents, exceeding 10 wt.-% (Fig. 5c). The variation of Al_2O_3 contents in the Methana amphiboles shows a bimodal distribution with maxima at 11 to 14 wt.-% and 7 to 10 wt.-% and many of the amphiboles with the high Al_2O_3 contents also have high Mg# >70 (Fig. 5c). The amphiboles in the volcanic rocks of Methana frequently show dark rims consisting of oxides, pyroxene and plagioclase. The $(La/Sm)_N$ of the amphiboles range from 0.4. to 1.4 (Fig. 6a) and the most light Rare Earth Element (REE) enriched amphibole crystals show a larger negative Eu-anomaly **compared to** amphiboles with lower $(La/Sm)_N$. Similarly, the amphibole Nb/La ratios show a negative trend with increasing $(La/Sm)_N$ (Fig. 6).

Olivine occurs as small subhedral (<1 mm) grains in both lavas and enclaves. In the enclaves and in andesites we find olivine with cores of Fo_{92-90} (Fig. 5a) and narrow rims with Fo_{78-80} but also homogeneous olivine with Fo_{86}. Clinopyroxene is abundant in the andesites and

enclaves but rare in dacites and occur typically as relatively small grains with <1mm diameter. The Mg# range **from** 90 **to** 70 but are more restricted between 88 and 75 **in most samples (Fig. 3d)**. The clinopyroxenes with high Mg# of 88 have high Cr_2O_3 contents up to 1 **wt.-%** but decrease with decreasing Mg# (Fig. 5b).

Biotite is abundant in many samples and occurs as elongated euhedral to anhedral crystals with sizes up to 5 mm; greenish clinopyroxene occurs in many samples and is typically euhedral with sizes up to 1 mm, whereas orthopyroxene is rare and grains are generally smaller. Oxides are commonly anhedral, larger and more common in the lavas compared to the enclaves. Magnetite and ilmenite **generally** occur in direct juxtaposition and have been used for thermobarometric calculations (see below). Magnetites have FeO contents of 71.1 to 87.6 wt.-%, while ilmenite displays TiO_2 contents between 22.6 to 47.1 wt.-% and FeO contents from 46.4 to 67.4 wt.-%. From the lavas containing both magnetite and ilmenite we calculated oxygen fugacities (fO_2) (Lepage, 2003, Spencer & Lindsley, 1981) and find a range from -13.5 to -6.7 for temperatures of 750 to 1200°C, corresponding to FMQ +1 to +2 (Fig. 7).

Chemical and isotopic composition of the whole rocks

The lavas from Methana range from calc-alkaline basaltic andesites and andesites to dacitic compositions whereas the enclaves are dominantly basaltic to basaltic andesitic in composition (Fig. 8a). All lavas and enclaves are classified as medium-K lavas with one exception (sample GZNME1518) and resemble previous data from Methana as well as lavas from Santorini and Nisyros in the eastern part of the Aegean arc (Fig. 1). The Methana enclaves and lavas lie along similar major element trends and display decreasing FeO^T and TiO_2 and increasing K_2O contents with increasing SiO_2. The enclaves generally have higher MgO contents of 7 to 3 wt.-% whereas the lavas typically have MgO concentrations of <4 wt.-% and SiO_2 of >57 wt.-% (Fig. 8e). The most mafic lavas of Methana are basaltic andesites from the Akri Pounda/Malisa

Volcano (sample locations 7 – 8 and 72 – 73, respectively in Fig. 1b) on the SW coast with ~55 wt.-% SiO_2 and 6 wt.-% MgO. The enclaves have variable Al_2O_3 contents whereas the lavas lie on a relatively tight decreasing trend with increasing SiO_2 (Fig. 8d). The Methana lavas and their enclaves both have increasing P_2O_5 from SiO_2 contents of 51 to 58 wt.-% but decreasing P_2O_5 contents at high SiO_2 (Fig. 8f). **They** follow similar major element trends **compared to** lavas from Nisyros whereas there is a notable distinction to the Santorini magmas that display increasing FeO^T and TiO_2 before decreasing at >58 wt.-% SiO_2. The major differences between the Methana and Nisyros rock suites are increased TiO_2 values **of** up to 1.2 wt.-% between 58 and 62 wt.-% SiO_2 and lower FeO^T values of 4.5 to 5.5 wt.-% between 54 and 58 wt.-% SiO_2 at Nisyros. Moreover, Nisyros **has** higher P_2O_5 contents which increase to ~0.25 wt.-% whereas the Methana lavas only show a maximum of ~0.15 wt.-% P_2O_5 (Fig. 8f).

The trace elements Sr and Zr show slightly increasing concentrations with increasing SiO_2 in the mafic Methana rocks (Fig. 9) but Sr decreases in lavas with >57 wt.-% SiO_2 whereas the Zr concentrations remain constant. Santorini lavas have lower Sr contents and those from Nisyros have higher Sr contents **compared to** the Methana samples. The mafic rocks from all three **Aegean arc** volcanic islands have similar Zr contents but the trend of the evolved samples from Santorini show a stronger increase **relative to** the two other volcanoes (Fig. 9b).

Chondrite-normalized $(La/Sm)_N$ **ratios** increase with increasing SiO_2 similar to the Nisyros lavas whereas a flatter trend is observed in the Santorini lavas (Fig. 10a). The Nb/Zr ratios in all lava suites in the Aegean arc are constant with variable SiO_2 (Fig. 10b). Methana lavas have higher Nb/Zr than lavas from Santorini that are similar to mid-ocean ridge basalts (MORB). The Ba/Th increase slightly in the evolved rocks but all samples of Methana, Santorini and Nisyros show a similar range in compositions between 20 and 140 (Fig. 10c). The Nd isotope ratios typically decrease with increasing SiO_2 contents in all lavas of the Aegean arc but enclaves with 50 wt.-% SiO_2 have relatively high Nd isotope ratios with the other

enclaves showing a decreasing trend with increasing SiO_2 (Fig. 10d). The lavas are more variable in **their** Nd isotope **composition** than enclaves and many of the samples with >56 wt.-% SiO_2 have $^{143}Nd/^{144}Nd$ <0.5125. The Eu anomaly remains relatively constant with increasing SiO_2 in lavas from Methana and Nisyros but becomes larger in the evolved lavas from Santorini (Fig. 10e). The Th/Nd ratios increase with increasing SiO_2 in the samples from Methana and Santorini from values slightly higher than MORB in the basalts to much higher Th/Nd in the evolved lavas. The Th/Nd of the most primitive lavas from Nisyros overlap MORB but the dacitic lavas also have much higher Th/Nd.

The $^{87}Sr/^{86}Sr$ ratios range from 0.70541 to 0.70840 and are significantly higher than most samples from Santorini and Nisyros in the central and eastern Aegean arc (Fig. 11a). Neodymium isotope ratios range from 0.51224 to 0.51266 and generally decrease with increasing $^{87}Sr/^{86}Sr$ (Fig. 11a). Several samples show relatively constant $^{143}Nd/^{144}Nd$ of ~0.5125 but variable Sr isotope ratios between 0.7060 and 0.7075 (Fig. 11a). The lavas with the highest Sr and lowest Nd isotope compositions overlap with the sediments recovered from drilled cores in the Hellenic Trench (Klaver *et al.*, 2015) but granites from the Aegean lie in the elongation of the trend of the Methana lavas (Fig. 11a). In terms of the Pb isotope ratios all Methana lavas are considerably higher in $^{207}Pb/^{204}Pb$ and $^{208}Pb/^{204}Pb$ for a given $^{206}Pb/^{204}Pb$ than MORB (Fig. 11c) and the lava compositions overlap with those of the sediments subducted along the Aegean arc. The Pb isotope ratios of the Methana lavas are higher than those of the volcanic rocks of Nisyros and most of Santorini. The Methana volcanic rocks have lower Nd isotopes than Santorini and Nisyros lavas but comparable ranges of $(La/Sm)_N$ and Th/Nd (Fig. 12). Both $(La/Sm)_N$ and Th/Nd show slightly decreasing $^{143}Nd/^{144}Nd$ with increasing element ratios.

DISCUSSION

Fractional crystallisation processes in the Methana magmas

Magmas ascending from the mantle through the continental crust stagnate at different levels where they may fractionate, mix, and assimilate, typically beginning in the lower crust (e.g. Annen *et al.*, 2006, Hildreth & Moorbath, 1988). The most mafic rocks from Methana are the enclaves with <52 wt.-% SiO_2 (Fig. 8) that have higher K_2O and lower FeO^T than basalts from Santorini (Bailey *et al.*, 2009, Nicholls, 1971). The mafic enclaves in the Methana lavas are relatively fine-grained and thus represent magma compositions rather than magma chamber cumulates. Woelki *et al.* (2018) suggested that the Fo-rich olivines in the Methana enclaves and lavas (up to Fo92) require primary magmas with Mg# ~72 and the high Mg# of the clinopyroxenes of up to 90 (Fig. 5b) also require a Mg-rich primary magma beneath Methana. The most mafic enclaves have an Mg# of ~65 implying considerable chemical evolution from the primary mantle magma. **Similar mafic enclaves are typical for the calc-alkaline magmas of the Aegean arc and other island arcs (e.g. Didier, 1973, Zellmer & Turner, 2007). Combining the lavas and the enclaves, clear compositional trends of major and trace elements occur versus SiO_2 (Figs. 8 and 9). The genetic relationship between the enclaves and the Methana lavas is supported by the continuous and overlapping trends of some incompatible element ratios like Nb/Zr and Ba/Th that are not extensively affected by the fractionating phases (Fig. 10).**

Extensive fractional crystallisation is also evident from the large compositional variation (e.g. An_{92} to An_{33}) and normal zoning of plagioclase and amphibole phenocrysts (Figs. 2 and 4) that **require crystallisation of the minerals either by simple cooling (e.g. de Silva *et al.*, 2008) or decompression along with degassing (e.g. Applegarth *et al.*, 2013) of the magma. Many plagioclase samples display plateaus at An_{70-80} and An_{35-50} and formed in magmas with**

basaltic to andesitic and dacitic to rhyolitic compositions, respectively (Nandedkar *et al.*, 2014). The plagioclase compositions likely reflect mixing between such magmas during the ascent thereby adding plagioclase with primitive cores to dacitic magmas. However, these plateaus are separated by 100 to 200 μm thick transitional zones (Fig. 2) indicating growth from melts with evolving compositions and the distribution of compositions is not bimodal but ~60% of the plagioclase analyses are in the range of 40 to 50% An (Fig. 3b). Additionally, the Methana plagioclase crystals do not show the bimodal Fe contents observed, for example, by Kent et al. (2010) in andesitic lavas from Mount Hood, Oregon. Most of the Methana plagioclase crystals have relatively low FeO contents <0.3 wt.-% at highly variable An contents between 30 and 90% (Fig. 5d). The FeO contents >0.3 wt.-% in plagioclase appear generally restricted to the An-rich crystals in more mafic magmas with >3 wt.-% MgO suggesting that there was little hybridization of the dacitic and basaltic magmas. Thus, although some magma mixing is indicated by the compositional plateaus, most of the variation in plagioclase is probably related to fractional crystallisation, particularly in the evolved andesitic to dacitic melts. The temperatures calculated for the magmas range from 1200 to 750°C (Fig. 7), implying a considerable cooling from the mafic to the dacitic melts (Fig. 8, 9). This range of temperatures is similar to that found in crystallisation experiments of calc-alkaline magmas (Blatter *et al.*, 2013, Nandedkar *et al.*, 2014).

It has been shown previously that trends in calc-alkaline lavas may not represent liquid lines of descent and that magma mixing and mineral accumulation affects the bulk composition of most rocks (e.g. Eichelberger *et al.*, 2006). Several elements like MgO and Al_2O_3 have highly variable concentrations especially in the Methana lavas with SiO_2 <57 wt.-% that probably indicate accumulation of mafic minerals and plagioclase. However, some elements like, for example, P and Sr show increasing concentrations between SiO_2 contents of 52 and 57 wt.-%

and decreasing concentrations at higher SiO_2 contents (Fig. 8f and 9c). The change in the trend of P_2O_5 (Fig. 8f) reflects the onset of apatite fractionation in the felsic magmas but disagrees with a model that the trends reflect binary mixing of mafic and felsic magmas (Elburg *et al.*, 2018). The compositional scatter along the trends allows perhaps 10% mixing of a mafic with a felsic end-member (Fig. 8f) but the felsic magmas with SiO_2 >60 wt.-% may reflect more extensive mixing with more mafic melts. Additionally, we do not exclude mixing across a smaller range of SiO_2, i.e. mixing between intermediate (<57 wt.-% SiO_2) and mafic (>52 wt.-% SiO_2), or intermediate and felsic (>57 wt.-% SiO_2) melts. We conclude that the major element trends for the Methana enclaves and lavas largely reflect fractional crystallisation processes of olivine, Cr-spinel, clinopyroxene, amphibole, plagioclase, and FeTi-oxides, but limited magma mixing and mineral accumulation caused considerable compositional variation along the trends.

The earliest fractionating phases at temperatures of ~1200°C are probably olivine, Cr-spinel, and clinopyroxene as indicated by decreasing Ni and Sc contents with increasing SiO_2 (Fig. 9) and in agreement with crystallisation experiments of primitive arc magmas (Pichavant & Macdonald, 2007, Sisson & Grove, 1993). Plagioclase crystallisation is suppressed by the high water contents and may occur below 1100°C (Pichavant & Macdonald, 2007). The decreasing Al_2O_3 and Sr concentrations at SiO_2 >57 wt.-% in the Methana lavas indicate plagioclase fractionation in the andesitic melts (Figs. 8d and 9c). Amphibole has the same effect as clinopyroxene on Sc but is not stable at temperatures >1000°C. Clinopyroxene cores are observed in some amphiboles in the Methana rocks and indicate that amphibole may form from clinopyroxene and olivine during cooling in the crust which has also been found in other volcanoes (Klaver *et al.*, 2017, Smith, 2014) and in experiments (Foden & Green, 1992). Most olivine grains are also anhedral and show signs of resorption and rims of orthopyroxene. These minerals are probably **xenocrystic** remnants of primitive early magmas similar to those observed in many subduction-related lavas (Kamenetsky *et al.*, 2001, Streck *et al.*, 2007).

Amphibole is abundant in the Methana lavas and amphibole fractionation has been suggested to be crucial for many subduction-related magmas (e.g. Davidson *et al.*, 2007, Larocque & Canil, 2010). Amphibole as fractionating phase can explain the increasing SiO_2 and $(La/Sm)_N$ **ratios** in the Methana lavas (Fig. 10a) because amphibole has lower SiO_2 and $(La/Sm)_N$ than the mafic magmas. The amphiboles in the Methana lavas show a variation between 0.4 and 1.5 in $(La/Sm)_N$ (Fig. 6) which most likely reflects variations in the magma compositions, i.e. crystallisation from variably light REE enriched melts. This variation is comparable to that observed in the cumulate amphiboles of Nisyros and the amphiboles from the high-Mg# andesites of the Adamello pluton (Klaver *et al.*, 2017, Tiepolo *et al.*, 2011). The most light REE enriched amphiboles have the lowest Eu/Eu* and Nb/La and thus, the enrichment in $(La/Sm)_N$ in the amphiboles probably indicates increasing crystal fractionation and Eu removal by plagioclase from the magma. The steep decrease of Nb/La with increasing $(La/Sm)_N$ in the amphibole may reflect the relative depletion of Nb relative to La in the magmas because of the higher D_{Nb} in amphibole (Tiepolo *et al.*, 2000). We conclude that the crystallisation and fractionation of amphibole leads to an enrichment of light REE and Nb relative to middle and heavy REE, i.e. amphibole fractionation has significant effects on incompatible element ratios in the evolved magmas (Davidson *et al.*, 2007, Dessimoz *et al.*, 2012). **Because amphibole crystallises relatively late from the Methana magmas we propose that the relatively low $(La/Sm)_N$ and Th/Nd but high $^{143}Nd/^{144}Nd$ of the mafic enclaves compared to the more evolved rocks (Fig. 10) indicate that the basalts closely resemble partial melts from the mantle wedge in terms of their incompatible element and Sr-Nd-Pb isotope ratios.**

In contrast to the abundant occurrence of amphibole and biotite in the Methana rocks and in the early lava series from Santorini, the younger Santorini lavas generally lack hydrous minerals (Nicholls, 1971). The absence of large amounts of amphibole (and biotite) in the

younger Santorini fractionation assemblage can explain the shallower trend of $(La/Sm)_N$ (Fig. 10a). This may either indicate crystallisation under hotter conditions (Klaver *et al.*, 2016), at lower pressure (Elburg *et al.*, 2014), or less volatiles in the Santorini than in the Methana magmas. The young Santorini magmas show an initial FeO enrichment with increasing SiO_2 which is different from the calc-alkaline trend of continuously decreasing FeO^T observed in the Methana magmas (Fig. 8c) but also from the early calc-alkaline lavas of Santorini (Nicholls, 1971). Experiments on Santorini basalt show that amphibole becomes stable at water contents >3.5 wt.-% (Andújar *et al.*, 2015) indicating that the young Santorini magmas are drier than the older magma series. This also suggests that the mafic Methana magmas have high water contents >3.5 wt.-% because amphibole crystallises early in these magmas. The lower CaO contents of olivine with Fo_{90} also supports more water in the Methana basalts compared to Santorini because there appears to be relation between the D_{Ca} in olivine and **H_2O** content of the parent melt (Gavrilenko *et al.*, 2016). The Methana olivines resemble the Ca-poor olivines from Klyuchevskoy and Shiveluch volcanoes in Kamchatka with **H_2O** contents of 4 to 6 wt.-% (Fig. 5a). Additionally, our amphibole temperature estimates **(765 to 1015°C (± 22°C) after Ridolfi et al. (2010))** show the same temperature range as calculations by Mortazavi and Sparks (2004) but result in slightly lower maximum temperatures than Santorini. In **agreement with previous work** (Andújar *et al.*, 2015) we suggest that the abundance of biotite and amphibole in Methana lavas in comparison to those from Santorini reflects higher **H_2O** contents of ~4 wt.-% in the primitive Methana magmas than in the Santorini melts.

Constraints on the oxidation state of ascending magmas

In the Methana enclaves and lavas, FeO^T and TiO_2 decrease between 52 and 65 wt.-% SiO_2 while the Santorini lavas and some from Nisyros show an increase in FeO^T from 50 to 56 wt.-% SiO_2 and then a decrease which is also observed in TiO_2 at SiO_2 <56 wt.-% (Fig. 8). Elburg et al. (2014) noted an earlier fractionation of oxides like Ti-magnetite and ilmenite in the

Methana melts compared to Santorini leading to stronger depletion of FeO^T and TiO_2 versus SiO_2 (Fig. 8). Moreover, the V concentrations of the Santorini samples are generally higher than those in the Methana magmas at corresponding SiO_2. The calculated oxygen fugacities (fO_2) (Lepage, 2003, Spencer & Lindsley, 1981) in the lavas containing both magnetite and ilmenite range from -13.5 to -6.7 for the range of 750 to 1200°C, corresponding to FMQ +1 to +2 (Fig. 7). The fO_2 calculated from the Methana oxides is higher than that of lavas from Santorini but comparable to rocks from Nisyros (Fig. 7) indicating more oxidizing conditions in the Methana magmas **compared to** the Santorini melts. This is also supported by differing trends of the Eu anomaly (Eu/Eu*) in the lavas which display a stronger decrease at Santorini compared to Methana and Nisyros (Fig. 10e). Plagioclase substitutes Sr, and Eu^{2+} for Ca but the incorporation of Eu into plagioclase depends on fO_2 (Drake, 1975). The decreasing Sr contents with increasing SiO_2 (Fig. 9c) imply that plagioclase fractionates in all three volcanic systems but is more abundant in the Santorini magmas. Some amphiboles of the Methana mafic enclave GZNME1589 lack an Eu-anomaly suggesting crystallisation of amphibole prior to plagioclase whereas the REE patterns of more evolved amphibole show a distinct Eu-anomaly (Fig. 6). However, the Eu/Eu* of Methana and Nisyros lavas remain nearly constant whereas there is a significant decrease with increasing SiO_2 in the Santorini lavas. This difference probably reflects the lower fO_2 in the Santorini magmas which lead to higher Eu^{2+}/Eu^{3+}. However, the Eu/Eu* ratios in plagioclase from Methana lavas range **from** 27 **to** 0.8 which is comparable to the range observed in Nisyros cumulates (Klaver *et al.*, 2017). This may imply that some plagioclase crystals formed in reducing magmas rather than in highly oxidized melts with little Eu^{2+}. The amphibole crystals from Methana lavas and enclaves and Nisyros cumulates also show a variation of the Eu/Eu* from 1.0 to 0.4 (Fig. 6a) reflecting the fractionation of plagioclase and magma evolution.

The differences of magma evolution between the western Aegean volcanoes and the younger Santorini lavas was noted by Nicholls (1971) who suggested that the young Santorini magmas contain less $\mathbf{H_2O}$ and are less oxidized than the melts of the western volcanoes, in agreement with our data. Experimental data on Santorini mafic magmas show that amphibole crystallisation requires water contents >3.5 wt.-% at fO_2 of FMQ+1 and temperatures of <975°C whereas the young Santorini magmas have lower water contents and fO_2 (Andújar *et al.*, 2015). The high Mg# of some amphibole crystals particularly in the mafic enclaves of Methana indicate crystallisation from mafic melts and therefore $\mathbf{H_2O}$ contents >3.5 wt.-%. The variable fO_2 in magmas may either reflect variations in the mantle source (e.g. sediment subduction), or variable processes (e.g. assimilation, fractional crystallisation, degassing) during the ascent of the magmas (Cottrell & Kelley, 2011, Grocke *et al.*, 2016, Lee *et al.*, 2005, Rowe *et al.*, 2009). Importantly, the mafic magmas from Methana with high temperatures of 1200°C display >FMQ+1 similar to the evolved lavas (Fig. 7) implying that the high fO_2 reflect the mantle source rather than processes during magma ascent. Such oxidized mantle may form due to the subduction of oxidized C and S in sedimentary components into the mantle wedge (Evans, 2012, Rielli *et al.*, 2017). The high fO_2 of the Methana basalts probably results from a higher sediment contribution compared to the eastern Aegean arc that causes, for example, lower $^{143}Nd/^{144}Nd$ than in Santorini basalts (Fig. 11) and was suggested by previous work (e.g. Elburg *et al.*, 2014, Francalanci *et al.*, 2005, Woelki *et al.*, 2018). We conclude that the variable subduction of sediments beneath the Aegean causes formation of relatively oxidized and water-rich primary magmas with the fO_2 and water content reflecting the variable composition and amount of recycled sediment.

Constraints on crustal stagnation levels of the Methana magmas

Basaltic melts did not erupt on Methana (Fig. 1) but apparently intruded into stagnant andesitic to dacitic magmas in crustal magma reservoirs and thus occur only as enclaves in the silicic

host rocks (Dietrich *et al.*, 1988, Elburg *et al.*, 2018). The Al content in amphibole in magmatic rocks has been widely used to calculate temperatures and pressures of crystallisation **and the H_2O content of the melt** (e.g. Costa *et al.*, 2013, Ridolfi & Renzulli, 2012) but the compositional variation in amphibole may also reflect mixing of magmas with different composition (e.g. Bachmann & Dungan, 2002, Erdmann *et al.*, 2014, Rutherford & Devine, 2003). Moreover, experimental work on amphibole from basaltic and andesitic melts of Santorini found large differences between pressures in experiments and those calculated from the amphibole compositions (Andújar *et al.*, 2015). The Methana amphibole compositions suggest a range of crystallisation temperatures from 765 to 1015°C (± 22°C) based on the method of Ridolfi *et al.* (2010) which is in the range of 750 to 1203°C (± 35°C) calculated using the ilmenite-magnetite thermometer of Spencer and Lindsley (1981) but limited by the upper stability of amphibole at temperatures of less than ~1050°C (Blatter *et al.*, 2013, Foden & Green, 1992). The high temperature and Mg# of some amphibole crystals suggest formation from mafic magma which is in general agreement with the occurrence of most amphiboles with Mg# >70 in mafic to intermediate rocks (>3 wt.-% MgO). We find that most amphiboles in **the** Methana lavas with MgO <3 wt.-% contain <10 wt.-% Al_2O_3 whereas amphiboles in the primitive enclaves with MgO >6 wt.-% have high Al_2O_3 of 11 to 14 wt.-% (Fig. 6c). Thus, there appears to be a relationship between amphibole and magma composition which could be due to amphibole crystallisation from different magmas or at different depths, or both **as well as different temperature or H_2O content of the melt**. **A similar variation was observed in amphiboles of cumulates from Nisyros by Klaver et al. (2017) who suggested that the high Al_2O_3 contents largely result from crystallisation at high pressures of** 0.5 to 0.8 GPa. Experiments on melts from Santorini with comparable compositions to those of Methana by Andujar *et al.* (2016) and Cadoux *et al.* (2014) show that amphibole with 7 to 12 wt.-% Al_2O_3 form at pressures of 0.2 to 0.4 GPa (Fig. 5c) and H_2O contents >4.5 wt.-%. Additionally,

equation 1c of Ridolfi and Renzulli (2012) yields amphibole crystallisation pressures with a bimodal distribution with average values of 0.16 and 0.38 ± **0.12** GPa (errors after Erdmann *et al.*, 2014). **The pressure estimates are affected by large errors of the amphibole barometry sometimes even resulting in negative pressures** (Erdmann *et al.*, 2014, Putirka, 2016). The crystallisation in the shallow crust at less than **15 km depth (<0.4 GPa)** beneath Methana is comparable to the situation at Santorini where mafic magmas appear to stagnate at depths of 15 to 12 km (Andújar *et al.*, 2016), whereas the felsic magmas generally reside in reservoirs between 10 and 2 km depth (Druitt *et al.*, 2016). On the other hand, the most mafic enclave GZNME 1549 with 7.2 wt.-% MgO contains amphibole with Al_2O_3 to 15 wt.-% (Fig. 5c) that resemble amphiboles from experiments on calc-alkaline melts at **0.7 to 0.9 GPa (Blatter *et al.*, 2013) corresponding to crystallisation depths higher than 25 km** which is comparable to the observations on mafic cumulates at Nisyros that formed at high pressures of 0.5 to 0.8 GPa, i.e. at 25 to 30 km depth (Klaver *et al.*, 2017). Most pressures indicated by the Methana amphiboles correspond to the intermediate to shallow crust that largely consists of metasedimentary rocks whereas the deep crystallisation occurred closer to the Moho lying at ~30 km underneath Methana (Tirel *et al.*, 2004). In conclusion, amphibole compositions indicate that fractional crystallisation in the magma system beneath Methana occurred at different levels in the crust with mafic magmas from the deeper part of the system ascending into the felsic magmas in the shallower crust. Such intrusion processes caused the formation of mafic enclaves and the reheating potentially triggered the ascent and eruption of the felsic magmas (e.g. Murphy *et al.*, 2000). Because the volumes of erupted magmas on Methana are **small (<<1 km^3)**, we believe that the mafic magmas intrude as dikes into small felsic magma reservoirs at different shallow crustal levels as suggested by Eichelberger et al. (2006).

Evidence for magma mixing

The abundance of rounded enclaves **and the presence of olivine xenocrysts** in the felsic Methana lavas probably reflects the intrusion of mafic magmas intruded into silicic magma **systems** beneath Methana. Whereas the enclaves typically show sharp boundaries to the surrounding **host lava**, i.e. no evidence of mixing, the textures and compositions of minerals imply either mixing between mafic and felsic melts, or that the different magmas picked up variable cumulate minerals during the ascent. For example, dacite GZNME1561 contains three populations of plagioclase (An85, 65 and 45) and amphibole (Mg# 64-70, 54-60, and 46-52; Fig. 3) that may indicate mixing of variable melts. Complex mixing relationships between melts and minerals are typical for lavas in continental subduction zones (Costa *et al.*, 2013, Eichelberger *et al.*, 2006, Streck & Leeman, 2018). The compositional trends of the Methana lavas have previously been interpreted to reflect binary mixing between basaltic andesite and a felsic melt possibly with >70 wt.-% SiO_2 (Elburg *et al.*, 2018). Such binary mixing leads to linear trends rather than the curved or kinked trends of Ni, Sr, and P_2O_5 versus SiO_2 in the Methana lavas (Figs. 8f and 9a). Thus, binary mixing between two extreme end-member compositions appears unlikely. However, the occurrence of clinopyroxene with high Mg#, of sieve-textured plagioclase (Fig. 2d), and the large range of plagioclase compositions between An_{45} and An_{90} in the andesitic and dacitic lavas (Figs. 2 and 3a) reflect interaction between basaltic magmas or their cumulates, and evolved melts. The recharge by mafic melt may cause increasing temperatures in the felsic magmas and partial dissolution of plagioclase phenocrysts (Andrews *et al.*, 2008) and the abrupt increase in An contents towards the rim (Fig. 2b). Such melt mixing leads to chemical and/or thermal disequilibrium resulting in the observed sieve textures of Ca-rich plagioclase (Tsuchiyama, 1985), partly embayed rims of felsic plagioclase, and dissolution of amphiboles (Fig. 2). Additionally, the presence of low and high Al-amphiboles with high Mg# in the andesitic and dacitic lavas (e.g. dacite GZNME1561, Fig. 3b)

indicates mixing of magmas with different compositions that **either** stagnated at different depths in the crust beneath Methana, **or generally had different temperatures or H_2O contents**. We suggest that the major and trace element trends argue against binary mixing between mafic and felsic magmas as main process forming the trends, but that limited mixing (<10%) of mafic magmas during intrusion into felsic magma may occur (Fig. 8f). The abundance of mafic enclaves in the felsic lavas indicates that there was little interaction possibly because of high viscosities of the magmas and rapid quenching of mafic magmas. **The mixing signatures commonly seen in mineral petrography and geochemistry might be caused by mixing of compositionally similar melts with different temperatures or H_2O contents as well as different water contents (Erdmann *et al.*, 2014).**

The most primitive enclave (Sample: GZNME1549) with 7.2 wt.-% MgO contains relatively homogeneous olivine with Fo_{87}, plagioclase with An-contents up to 90, and amphiboles with Mg# up to 74 and Al_2O_3 contents up to 15.8 wt.-% (Figs. 3 and 5). Other MgO-rich enclaves contain olivine with Fo_{91} implying that these mafic magmas carried the mafic minerals into the felsic magmas. The large variation of olivine with Fo contents between 78 and 92 and plagioclase An between 44 and 90 within the mafic enclaves (Figs. 3 and 5) implies that they also formed by mixing processes prior to intruding into the felsic magma reservoirs. The ascent of the mafic magmas into the shallow felsic reservoirs may have been triggered by an extensional tectonic phase which in turn caused eruption of the felsic melts (Elburg *et al.*, 2018).

We conclude that complex processes of fractional crystallisation and mixing occurred at several levels in the Methana magma system and that small batches of melt interacted with each other. Such processes appear to be typical for magma systems at active continental margins (Costa *et al.*, 2013, Erdmann *et al.*, 2014, Kent *et al.*, 2010).

The effect of assimilation of crustal rocks on the Methana magma compositions

The mantle wedge beneath the Aegean arc is affected by sediment subduction but the magmas ascending into the crust additionally assimilate sedimentary material (Bailey *et al.*, 2009, Elburg *et al.*, 2014, Woelki *et al.*, 2018). For example, Elburg *et al.* (2014) proposed that the Sr and Nd isotope trends in the Methana lavas are the result of two mixing stages, where the first stage involves sediment subduction into the mantle, and the second stage involves assimilation of crustal rocks. The Methana enclaves and lavas show increasing Th/Nd but generally decreasing $^{143}Nd/^{144}Nd$ with increasing SiO_2, and Aegean I- and S-type granites form an extension of the trends of the Methana lavas (Fig. 10d and f). These granites largely represent partial melts of metasediments (Altherr & Siebel, 2002, Juteau *et al.*, 1986, Pe-Piper, 2000, Stouraiti *et al.*, 2010) and thus probably resemble the crustal component in the Methana magmas. Simple binary mixing between a granitic end-member and a primitive Methana basalt suggests that the evolved Methana magmas may contain between 10 and 50% crustal melt (Fig. 10d). The crust beneath Methana has a thickness of ~30 km which is thicker than beneath the Aegean arc volcanoes further to the east where extension has reduced the crustal thickness to ~25 km (Tirel *et al.*, 2004). Seismic anisotropy studies suggest that the upper 10 km of the crust consist of metasediments whereas the lower 20 km of the crust consist of dense mafic rocks (Cossette *et al.*, 2016). The western Aegean crust of the Argolis Peninsula is part of the Subpelagonian Zone of the Hellenides and consists of a Palaeozoic basement with an upper crust of accreted Cretaceous to Eocene limestones and terrigenous flysch sediments (Faupl *et al.*, 1999, Robertson *et al.*, 1991). Similar Mesozoic metasediments are abundant on many Aegean islands and partial melting of these largely contributes to the Aegean granites (Altherr & Siebel, 2002, Pe-Piper, 2000, Stouraiti *et al.*, 2010) but also affects the Methana magmas (Figs. 10 and 11). The Methana lavas display two trends of $^{87}Sr/^{86}Sr$ versus $^{143}Nd/^{144}Nd$ where one trend shows increasing Sr and decreasing Nd isotope ratios and the other increasing

$^{87}Sr/^{86}Sr$ at constant $^{143}Nd/^{144}Nd$ (Fig. 11a). Although the lavas with the most radiogenic Sr isotope ratios overlap with the compositions of the Neogene sediments drilled in the Hellenic Trench (Fig. 11) we suggest that these Methana magmas with low $^{143}Nd/^{144}Nd$ assimilate Mesozoic metasediments because they generally have higher $^{208}Pb/^{204}Pb$ for a given $^{206}Pb/^{204}Pb$ **compared to** the young sediments but comparable to Aegean granite (Fig. 11c). Only the Methana samples with relatively high $^{143}Nd/^{144}Nd$ of 0.5125 but variable Sr isotope ratios (Fig. 11a) may have assimilated younger sediments. The significant assimilation of sedimentary material implies that these processes occur within the upper 10 km of the crust rather than in the lower crust that is probably composed of mafic igneous and metamorphic rocks (Cossette *et al.*, 2016). We conclude that most of the primitive Methana magmas mixed with partial melts of metasediments with low Nd and high $^{208}Pb/^{204}Pb$ isotope compositions but some Methana melts were also affected by younger sediments with relatively high $^{143}Nd/^{144}Nd$. The relatively high $^{143}Nd/^{144}Nd$ and high Al contents in the amphiboles of the mafic enclaves suggest that mafic magmas probably stagnated at ~14 km depth and assimilated less crustal material than the silicic melts represented by the lavas**. The lower An contents of plagioclase and Mg# of amphibole in the dacitic lavas compared to the mafic enclaves (Fig. 3) probably reflect the more extensive fractional crystallisation associated with assimilation in the evolved melts.**

We used the EC-RAFC model of Bohrson and Spera (2003) to estimate the assimilation and fractional crystallisation processes (Figs. 11 and 12) assuming magma temperatures of 1250 to 850°C (Fig. 7). The temperature in the crust beneath Methana is relatively high and estimates from hydrothermal fluids yield temperatures of 150°C in the shallow crust (Dotsika *et al.*, 2009) so that we assume a temperature of 400°C at 10 km depth. For the starting composition of the Methana mafic magma we **take** Sr and Nd isotope ratios of 0.7055 and 0.51265 (Table 3) that represent magma forming from a mixture between depleted MORB mantle (DMM) and sediment melt (Woelki *et al.*, 2018). The crustal end-member is defined by

the composition of Aegean granites with $^{87}Sr/^{86}Sr$ and $^{143}Nd/^{144}Nd$ of 0.7115 and 0.5121 because these granites are partial melts of the Aegean crust. Figure 11 shows the curves of the EC-RAFC model and in general there is a reasonable fit to the trend of most samples from Methana. The variation of the Pb isotopes indicates that there is considerable variation in the endmembers. The model suggests 72% fractional crystallisation and 40% assimilation for the most extreme Methana lavas at a temperature of 945°C (Figs. 11 and 12) which is supported by the temperature estimates from the oxide thermometry. Our calculations indicate a predominant trend of sediment contribution at Methana and the evolved lavas show an increased sediment contribution compared to the more primitive lavas represented in the form of enclaves. The curved variation of the Th/Nd ratio with decreasing Nd isotope ratios observed in the Methana lavas (Fig. 12b) is not fully reproduced but this may reflect the heterogeneity of the metasediments in the upper crust that is also displayed in the variation of Nd isotopes versus SiO_2 (Fig. 10f). The variation of the Th/Nd ratio reflects the fact that during fractional crystallisation Th is more incompatible than Nd and thus becomes relatively enriched, whereas at a later stage assimilation of a melt from metasediments with a Th/Nd of ~0.2 leads to decreasing Th/Nd (Fig. 12b). Thus, the chemical and isotopic variation observed in the relatively evolved magmas of Methana reflects extensive fractional crystallisation and assimilation of metasediments in the upper crust. There is little evidence for long residence of the mafic melts with assimilation in the lower crust beneath Methana.

CONCLUSIONS

The geochemistry and petrology of lavas and their enclaves of Methana peninsula show the impact of sediment subduction and assimilation on magma composition in an island arc setting. The basaltic primary melts indicate metasomatism by sediment melts from the subducting slab but the ascending magmas also react with the metasedimentary rocks of the accreted crust in

the Aegean. **The variation of amphibole compositions and comparison with experimental results** indicate stagnation of the melts at **a range of** depths **from** the deep to shallow crust and cooling from more than 1200°C to about 800°C yielding andesitic and dacitic compositions. The basaltic magmas stagnate close to the Moho (~25 km) where they evolve by fractional crystallisation and minor assimilation. Significant contamination by metasediments associated by further crystallisation **mainly** occurs in the upper crust (<15 km depth) beneath Methana results in evolved magmas of predominantly andesitic to dacitic in composition. Both mafic and felsic Methana magmas have fO_2 of FMQ +1 to +2 that is much higher than that observed in Santorini melts and probably reflects the much stronger input of sediments into the mantle wedge whereas there is no systematic change during assimilation and fractional crystallisation processes. The eruption of the felsic magmas may be caused by the intrusion of more mafic magmas that now exist as enclaves in the felsic rocks. The occurrence of exclusively effusive eruptions at Methana as opposed to the large explosive eruptions observed in the eastern Aegean islands possibly results from efficient degassing and a low ascent rate through a relatively thicker crustal lid in the western Aegean.

ACKNOWLEDGEMENTS

We thank F. Kemner and T. Günther for help with the microprobe work and M. Hertel for help with the XRF analyses. This project was funded by the Deutsche Forschungsgemeinschaft (DFG) through grant HA 2568/33-1. We acknowledge logistic and field support by R. Romer, P. Nomikou, I. Smet, T. Pfeiffer, T. Schorr, C. Ats, M. Ythos, and F. Gold. We acknowledge the constructive comments by G. Cooper, M. Klaver, S. Erdmann, and M. Elburg that considerably improved the quality of this work.

REFERENCES

Altherr, R. & Siebel, W. (2002). I-type plutonism in a continental back-arc setting: Miocene granitoids and monzonites from the central Aegean Sea, Greece. *Contributions to Mineralogy and Petrology* 143, 397-415.

Andrews, B. J., Gardner, J. E. & Housh, T. B. (2008). Repeated recharge, assimilation, and hybridization in magmas erupted from El Chichón as recorded by plagioclase and amphibole phenocrysts. *Journal of Volcanology and Geothermal Research* 175, 415-426.

Andújar, J., Scaillet, B., Pichavant, M. & Druitt, T. H. (2015). Differentiation conditions of a basaltic magma from Santorini, and its bearing on the production of andesite in arc settings. *Journal of Petrology* 56, 765-794.

Andújar, J., Scaillet, B., Pichavant, M. & Druitt, T. H. (2016). Generation Conditions of Dacite and Rhyodacite via the Crystallization of an Andesitic Magma. Implications for the Plumbing System at Santorini (Greece) and the Origin of Tholeiitic or Calc-alkaline Differentiation Trends in Arc Magmas. *Journal of Petrology* 57, 1887-1920.

Annen, C., Blundy, J. D. & Sparks, R. S. J. (2006). The genesis of intermediate and silicic magmas in deep crustal hot zones. *Journal of Petrology* 47, 505-539.

Applegarth, L., Tuffen, H., James, M. & Pinkerton, H. (2013). Degassing-driven crystallisation in basalts. *Earth-Science Reviews* 116, 1-16.

Bachmann, O. & Dungan, M. A. (2002). Temperature-induced Al-zoning in hornblendes of the Fish Canyon magma, Colorado. *American Mineralogist* 87, 1062-1076.

Bailey, J. C., Jensen, E. S., Hansen, A., Kann, A. D. J. & Kann, K. (2009). Formation of heterogeneous magmatic series beneath North Santorini, South Aegean island arc. *Lithos* 110, 20-36.

Barton, M. & Huijsmans, J. P. P. (1986). Post-caldera dacites from the Santorini volcanic complex, Aegean Sea, Greece: an example of the eruption of lavas of near-constant composition over a 2,200 year period. *Contributions to Mineralogy and Petrology* 94, 472-495.

Beier, C., Brandl, P. A., Lima, S. L. & Haase, K. M. (2018). Tectonic control on the genesis of magmas in the New Hebrides arc (Vanuatu). *Lithos* 312-313, 290-307.

Blatter, D. L., Sisson, T. W. & Hankins, W. B. (2013). Crystallization of oxidized, moderately hydrous arc basalt at mid- to lower-crustal pressures: implications for andesite genesis. *Contributions to Mineralogy and Petrology* 166, 861-886.

Bohrson, W. A. & Spera, F. J. (2003). Energy-constrained open-system magmatic processes IV: Geochemical, thermal and mass consequences of energy-constrained recharge, assimilation and fractional crystallization (EC-RAFC). *Geochemistry, Geophysics, Geosystems* 4.

Braschi, E., Francalanci, L. & Vougioukalakis, G. E. (2012). Inverse differentiation pathway by multiple mafic magma refilling in the last magmatic activity of Nisyros Volcano, Greece. *Bulletin of Volcanology* 74, 1083-1100.

Buettner, A., Kleinhanns, I. C., Riufer, D., Hunziker, J. C. & Villa, I. M. (2005). Magma generation at the easternmost section of the Hellenic arc: Hf, Nd, Pb and Sr isotope geochemistry of Nisyros and Yali volcanoes (Greece). *Lithos* 83, 29-46.

Cadoux, A., Scaillet, B., Druitt, T. H. & Deloule, E. (2014). Magma storage conditions of large Plinian eruptions of Santorini Volcano (Greece). *Journal of Petrology* 55, 1129-1171.

Cassidy, M., Manga, M., Cashman, K. & Bachmann, O. (2018). Controls on explosive-effusive volcanic eruption styles. *Nature Communications* 9, 2839.

Clift, P. D. & Vannucchi, P. (2004). Controls on tectonic accretion versus erosion in subduction zones: Implications for the origin and recycling of the continental crust. *Reviews of Geophysics* 42.

Cossette, E., Audet, P., Schneider, D. & Grasemann, B. (2016). Structure and anisotropy of the crust in the Cyclades, Greece, using receiver functions constrained by in situ rock textural data. *Journal of Geophysical Research* 121, 2661-2678.

Costa, F., Andreastuti, S., Bouvet de Maisonneuve, C. & Pallister, J. S. (2013). Petrological insights into the storage conditions, and magmatic processes that yielded the centennial 2010 Merapi explosive eruption. *Journal of Volcanology and Geothermal Research* 261, 209-235.

Cottrell, E., Gardner, J. E. & Rutherford, M. J. (1999). Petrologic and experimental evidence for the movement and heating of the pre-eruptive Minoan rhyodacite (Santorini, Greece). *Contributions to Mineralogy and Petrology* 135, 315-331.

Cottrell, E. & Kelley, K. A. (2011). The oxidation state of Fe in MORB glasses and the oxygen fugacity of the upper mantle. *Earth and Planetary Science Letters* 305, 270-282.

Davidson, J., Turner, S., Handley, H., Macpherson, C. & Dosseto, A. (2007). Amphibole "sponge" in arc crust? *Geology* 35, 787-790.

Davidson, J. P. (1987). Crustal contamination versus subduction zone enrichment: Examples from the Lesser Antilles and implications for mantle source compositions of island arc volcanic rocks. *Geochimica et Cosmochimica Acta* 51, 2185-2198.

de Silva, S., Salas, G. & Schubring, S. (2008). Triggering explosive eruptions—The case for silicic magma recharge at Huaynaputina, southern Peru. *Geology* 36, 387-390.

de Voogd, B., Truffert, C., Chamot-Rooke, N., Huchon, P., Lallemant, S. & Le Pichon, X. (1992). Two-ship deep seismic soundings in the basins of the Eastern Mediterranean Sea (Pasiphae cruise). *Geophysical Journal International* 109, 536-552.

Dessimoz, M., Müntener, O. & Ulmer, P. (2012). A case for hornblende dominated fractionation of arc magmas: the Chelan Complex (Washington Cascades). *Contributions to Mineralogy and Petrology* 163, 567-589.

Didier, J. (1973). *Granites and their enclaves: the bearing of enclaves on the origin of granites*.

Dietrich, V. & Gaitanakis, P. (1995). Geological map of Methana peninsula (Greece). ETH Zürich, Switzerland.

Dietrich, V. J., Mercolli, I. & Oberhänsli, R. (1988). Dazite, High-Alumina-Basalte und Andesite als Produkte amphiboldominierter Differentiation (Aegina und Methana, Ägäischer Inselbogen). *Schweizerische Mineralogische und Petrographische Mitteilungen* 68, 21-39.

Dotsika, E., Poutoukis, D., Michelot, J. L. & Raco, B. (2009). Natural tracers for identifying the origin of the thermal fluids emerging along the Aegean Volcanic arc (Greece): Evidence of Arc-Type Magmatic Water (ATMW) participation. *Journal of Volcanology and Geothermal Research* 179, 19-32.

Drake, M. J. (1975). The oxidation state of europium as an indicator of oxygen fugacity *Geochimica et Cosmochimica Acta* 39, 55-64.

Druitt, T. H., Mercier, M., Florentin, L., Deloule, E., Cluzel, N., Flaherty, T., Médard, E. & Cadoux, A. (2016). Magma storage and extraction associated with Plinian and Interplinian activity at Santorini Caldera (Greece). *Journal of Petrology* 57, 461-494.

Eichelberger, J. C. (1995). Silicic volcanism: Ascent of viscous magmas from crustal reservoirs. *Annual Reviews of Earth and Planetary Sciences* 23, 41-63.

Eichelberger, J. C., Izbekov, P. E. & Browne, B. L. (2006). Bulk chemical trends at arc volcanoes are not liquid lines of descent. *Lithos* 87, 135-154.

Elburg, M. A., Smet, I. & de Pelsmaeker, E. (2014). Influence of source materials and fractionating assemblage on magmatism along the Aegean Arc, and implications for crustal growth. In: Gómez-Tuena, A., Straub, S. M. & Zellmer, G. F. (eds.) *Orogenic andesites and crustal growth*: Geol. Soc. London, Spec. Publ., 137-160.

Elburg, M. A., Smet, I., Van den haute, P., Vanhaecke, F., Klaver, M. & Andersen, T. (2018). Extreme isotopic variation documents extensional tectonics in arc magmas from Methana, Greece. *Lithos* 318-319, 386-398.

Erdmann, S., Martel, C., Pichavant, M. & Kushnir, A. (2014). Amphibole as an archivist of magmatic crystallization conditions: problems, potential, and implications for inferring magma storage prior to the paroxysmal 2010 eruption of Mount Merapi, Indonesia. *Contributions to Mineralogy and Petrology* 167, 1-23.

Evangelidis, C. P. (2017). Seismic anisotropy in the Hellenic subduction zone: Effects of slab segmentation and subslab mantle flow. *Earth and Planetary Science Letters* 480, 97-106.

Evans, K. A. (2012). The redox budget of subduction zones. *Earth-Science Reviews* 113, 11-32.

Fabbro, G., Druitt, T. H. & Scaillet, S. (2013). Evolution of the crustal magma plumbing system during the build-up to the 22-ka caldera-forming eruption of Santorini (Greece). *Bulletin of Volcanology* 75, 767.

Faupl, P., Pavlopoulos, A. & Migiros, G. (1999). The Paleogene history of the Pelagonian zone SL (Hellenides, Greece): Heavy mineral study from terrigenous flysch sediments. *Geologica Carpathica* 50, 449-458.

Foden, J. H. & Green, D. H. (1992). Possible role of amphibole in the origin of andesite: some experimental and natural evidence. *Contributions to Mineralogy and Petrology* 109, 479-493.

Francalanci, L., Varekamp, J. C., Vougioukalakis, G., Defant, M. J., Innocenti, F. & Manetti, P. (1995). Crystal retention, fractionation and crustal assimilation in a convecting magma chamber, Nisyros Volcano, Greece. *Bulletin of Volcanology* 56, 601-620.

Francalanci, L., Vougioukalakis, G. E., Perini, G. & Manetti, P. (2005). A west-east traverse along the magmatism of the south Aegean volcanic arc in the light of volcanological, chemical and isotope data. In: Fytikas, M. & Vougioukalakis, G. E. (eds.) *The South Aegean active volcanic arc: Present knowledge and future perspectives*: Elsevier, 65-111.

Freund, S., Beier, C., Krumm, S. & Haase, K. M. (2013). Oxygen isotope evidence for the formation of andesitic-dacitic magmas from the fast-spreading Pacific-Antarctic Rise by assimilation-fractional crystallization. *Chemical Geology* 347, 271-283.

Fytikas, M., Innocenti, F., Manetti, P., Mazzuoli, R., Peccerillo, A. & Villari, L. (1984). Tertiary to Quaternary evolution of volcanism in the Aegean region. In: Dixon, J. E. & Robertson, A. H. F. (eds.) *The geological evolution of the Eastern Mediterranean*: Geol. Soc. London Spec. Publ., 687-699.

Gavrilenko, M., Herzberg, C., Vidito, C., Carr, M. J., Tenner, T. & Ozerov, A. (2016). A calcium-in-olivine geohygrometer and its application to subduction zone magmatism. *Journal of Petrology* 57, 1811-1832.

Gill, J. B. (1981). *Orogenic andesites and plate tectonics*. Berlin: Springer.

Grocke, S. B., Cottrell, E., de Silva, S. & Kelley, K. A. (2016). The role of crustal and eruptive processes versus source variations in controlling the oxidation state of iron in Central Andean magmas. *Earth and Planetary Science Letters* 440, 92-104.

Grove, T. L., Till, C. B. & Krawczynski, M. J. (2012). The role of H_2O in subduction zone magmatism. *Annual Review of Earth and Planetary Sciences* 40, 413-439.

Haase, K. M., Beier, C., Regelous, M., Rapprich, V. & Renno, A. (2017). Spatial variability of source composition an petrogenesis in rift and rift flank alkaline lavas from the Eger Rift, Central Europe. *Chemical Geology* 455, 304-314.

Halpaap, F., Rondenay, S. & Ottemöller, L. (2018). Seismicity, deformation, and metamorphism in the western Hellenic Subduction Zone: New constraints from tomography. *Journal of Geophysical Research* 123.

Hildreth, W. & Moorbath, S. (1988). Crustal contributions to arc magmatism in the Andes of Central Chile. *Contributions to Mineralogy and Petrology* 98, 455-489.

Hofmann, A. W. (1988). Chemical differentiation of the Earth: the relationship between mantle, continental crust, and oceanic crust. *Earth and Planetary Science Letters* 90, 297-314.

Huijsmans, J. P. P. (1985). Calc-alkaline lavas from the volcanic complex of Santorini, Aegean Sea, Greece: a petrological, geochemical and stratigraphic study. Instituut voor Aardwetenschappen Rijksuniversiteit Utrecht.

Innocenti, F., Manetti, P., Peccerillo, A. & Poli, G. (1981). South Aegean volcanic arc: geochemical variations and geotectonic implications. *Bulletin of Volcanology* 44-3, 377-391.

Jolivet, L., Faccenna, C., Huet, B., Labrousse, L., Le Pourhiet, L., Lacombe, O., Lecomte, E., Burov, E., Denèle, Y., Brun, J.-P., Philippon, M., Paul, A., Salaün, G., Karabulut, H., Piromallo, C., Monié, P., Gueydan, F., Okay, A. I., Oberhänsli, R., Pourteau, A., Augier, R., Gadenne, L. & Driussi, O. (2013). Aegean tectonics: Strain localisation, slab tearing and trench retreat. *Tectonophysics* 597-598, 1-33.

Juteau, M., Michard, A. & Albarede, F. (1986). The Pb-Sr-Nd isotope geochemistry of some recent circum-Mediterranean granites. *Contributions to Mineralogy and Petrology* 92, 331-340.

Kamenetsky, V. S., Crawford, A. J. & Meffre, S. (2001). Factors controlling chemistry of magmatic spinel: an empirical study of associated olivine, Cr-spinel and melt inclusions from primitive rocks. *Journal of Petrology* 42, 655-671.

Kelemen, P. B. (1995). Genesis of high Mg# andesites and the continental crust. *Contributions to Mineralogy and Petrology* 120, 1-19.

Kent, A. J. R., Darr, C., Koleszar, A. M., Salisbury, M. J. & Cooper, K. M. (2010). Preferential eruption of andesitic magmas through recharge filtering. *Nature Geoscience* 3, 631-636.

Kirchenbaur, M., Münker, C., Schuth, S., Garbe-Schönberg, D. & Marchev, P. (2011). Tectonomagmatic constraints on the sources of Eastern Mediterranean K-rich Lavas. *Journal of Petrology* 53, 27-65.

Klaver, M., Carey, S., Nomikou, P., Smet, I., Godelitsas, A. & Vroon, P. (2016). A distinct source and differentiation history for Kolumbo submarine volcano, Santorini volcanic field, Aegean arc. *Geochemistry, Geophysics, Geosystems* 17.

Klaver, M., Djuly, T., de Graaf, S., Sakes, A., Wijbrans, J., Davies, G. & Vroon, P. (2015). Temporal and spatial variations in provenance of Eastern Mediterranean Sea sediments: Implications for Aegean and Aeolian arc volcanism. *Geochimica et Cosmochimica Acta* 153, 149-168.

Klaver, M., Matveev, S., Berndt, J., Lissenberg, C. J. & Vroon, P. Z. (2017). A mineral and cumulate perspective to magma differentiation at Nisyros volcano, Aegean arc. *Contributions to Mineralogy and Petrology* 172.

Kokinou, E., Kamperis, E., Vafidis, A., Monopolis, D., Ananiadis, G. & Zelilidis, A. (2005). Deep seismic reflection data from offshore Western Greece: A new crustal model for the Ionian Sea. *Journal of Petroleum Geology* 28, 185-202.

Kopf, A., Mascle, J. & Klaeschen, D. (2003). The Mediterranean Ridge: A mass balance across the fastest growing accretionary complex on Earth. *Journal of Geophysical Research* 108.

Kushiro, I. (1974). Melting of hydrous upper mantle and possible generation of andesitic magma: An approach from synthetic systems. *Earth and Planetary Science Letters* 22, 294-299.

Labanieh, S., Chauvel, C., Germa, A. & Quidelleur, X. (2012). Martinique: a clear case for sediment melting and slab dehydration as a function of distance to the trench. *Journal of Petrology* 53, 2441-2464.

Larocque, J. & Canil, D. (2010). The role of amphibole in the evolution of arc magmas and crust: the case from the Jurassic Bonanza arc section, Vancouver Island, Canada. *Contributions to Mineralogy and Petrology* 159, 475-492.

Le Maitre, R. W., Bateman, P., Dudek, A., Keller, J., LeBas, M. J., Sabine, P. A., Schmid, R., Sorensen, H., Streckeisen, A., Woolley, A. R. & Zanettin, B. (1989). *A classification of igneous rocks and glossary of terms*. Oxford: Blackwell.

Lee, C. T. A., Leeman, W. P., Canil, D. & Li, Z.-X. A. (2005). Similar V/Sc systematics in MORB and arc basalts: Implications for the oxygen fugacities of their mantle source regions. *Journal of Petrology* 46, 2313-2336.

Lepage, L. D. (2003). ILMAT: an Excel worksheet for ilmenite–magnetite geothermometry and geobarometry. *Computers & Geosciences* 29, 673-678.

Matsuda, J.-I., Senoh, K., Maruoka, T., Sato, H. & Mitropoulos, P. (1999). K-Ar ages of the Aegean volcanic rocks and their implication for the arc-trench system. *Geochemical Journal* 33, 369-377.

McClusky, S., Balassani, S., Barka, A., Demir, C., Ergintasv, S., Georgiev, I., Gurkan, O., Hamburger, M., Hurst, K., Kahle, H., Kastens, K., Kekelidze, G., King, R., Kotzev, V., Lenk, O., Mahmoud, S., Mishin, A., Nadariya, M., Ouzounis, A., Paradissis, D., Peter, Y., Prilepin, M., Reilinger, R., Sanli, I., Seeger, H., Tealeb, A., Toksöz, M. N. & Veis, G. (2000). GPS constraints on plate kinematics and dynam- ics in the eastern Mediterranean and Caucasus. *Journal of Geophysical Research* 105, 5695-5719.

McCulloch, M. T. & Gamble, J. A. (1991). Geochemical and geodynamical constraints on subduction zone magmatism. *Earth and Planetary Science Letters* 102, 358-374.

McCulloch, M. T., Kyser, T. K., Woodhead, J. D. & Kinsley, L. (1994). Pb-Sr-Nd-O isotopic constraints on the origin of rhyolites from the Taupo Volcanic Zone of New Zealand: evidenc for assimilation followed by fractionation from basalt. *Contributions to Mineralogy and Petrology* 115, 303-312.

Mortazavi, M. & Sparks, R. (2004). Origin of rhyolite and rhyodacite lavas and associated mafic inclusions of Cape Akrotiri, Santorini: the role of wet basalt in generating calcalkaline silicic magmas. *Contributions to Mineralogy and Petrology* 146, 397-413.

Murphy, M. D., Sparks, R. S. J., Barclay, J., Carroll, M. R. & Brewer, T. S. (2000). Remobilization of andesite magma by intrusion of mafic magma at the Soufriere Hills Volcano, Montserrat, West Indies. *Journal of Petrology* 41, 21-42.

Nandedkar, R. H., Ulmer, P. & Müntener, O. (2014). Fractional crystallization of primitive, hydrous arc magmas: an experimental study at 0.7 GPa. *Contributions to Mineralogy and Petrology* 167.

Nicholls, I. A. (1971). Petrology of Santorini Volcano, Cyclades, Greece. *Journal of Petrology* 12, 67-119.

Pe, G. G. (1974). Volcanic rocks of Methana, South Aegean Arc, Greece. *Bulletin of Volcanology* 38, 270-290.

Pe-Piper, G. (2000). Origin of S-type granites coeval with I-type granites in the Hellenic subduction system, Miocene of Naxos, Greece. *European Journal of Mineralogy* 12, 859-875.

Pe-Piper, G. & Piper, D. J. W. (2013). The effect of changing regional tectonics on an arc volcano: Methana, Greece. *Journal of Volcanology and Geothermal Research* 260, 146-163.

Pearce, F. D., Rondenay, S., Sachpazi, M., Charalampakis, M. & Royden, L. H. (2012). Seismic investigation of the transition from continental to oceanic subduction along the western Hellenic Subduction Zone. *Journal of Geophysical Research* 117, B07306.

Pearce, N. J., Perkins, W. T., Westgate, J. A., Gorton, M. P., Jackson, S. E., Neal, C. R. & Chenery, S. P. (1997). A compilation of new and published major and trace element data for NIST SRM 610 and NIST SRM 612 glass reference materials. *Geostandards newsletter* 21, 115-144.

Pichavant, M. & Macdonald, R. (2007). Crystallization of primitive basaltic magmas at crustal pressures and genesis of the calc-alkaline igneous suite: experimental evidence from St Vincent, Lesser Antilles arc. *Contributions to Mineralogy and Petrology* 154, 535-558.

Plank, T. & Langmuir, C. H. (1993). Tracing trace elements from sediment input to volcanic output at subduction zones. *Nature* 362, 739-743.

Price, R. C., Gamble, J. A., Smith, I. E. M., Stewart, R. B., Eggins, S. & Wright, I. C. (2005). An integrated model for the temporal evolution of andesites and rhyolites and crustal development in New Zealand´s North Island. *Journal of Volcanology and Geothermal Research* 140, 1-24.

Putirka, K. (2016). Amphibole thermometers and barometers for igneous systems and some implications for eruption mechanisms of felsic magmas at arc volcanoes. *American Mineralogist* 101, 841-858.

Reubi, O. & Blundy, J. D. (2009). A dearth of intermediate melts at subduction zone volcanoes and the petrogenesis of arc andesites. *Nature* 461, 1269-1273.

Ridolfi, F. & Renzulli, A. (2012). Calcic amphiboles in calc-alkaline and alkaline magmas: thermobarometric and chemometric empirical equations valid up to 1,130°C and 2.2 GPa. *Contributions to Mineralogy and Petrology* 163, 877-895.

Ridolfi, F., Renzulli, A. & Puerini, M. (2010). Stability and chemical equilibrium of amphibole in calc-alkaline magmas: an overview, new thermobarometric formulations and application to subduction-related volcanoes. *Contributions to Mineralogy and Petrology* 160, 45-66.

Rielli, A., Tomkins, A. G., Nebel, O., Brugger, J., Etschmann, B., Zhong, R., Yaxley, G. M. & Paterson, D. (2017). Evidence of sub-arc mantle oxidation by sulphur and carbon. *Geochemical Perspectives* 3, 124-132.

Robertson, A., Clift, P., Degnan, P. & Jones, G. (1991). Palaeogeographic and palaeotectonic evolution of the Eastern Mediterranean Neotethys. *Palaeogeography, Palaeoclimatology, Palaeoecology* 87, 289-343.

Robertson, A. H. F. (2004). Development of concepts concerning the genesis and emplacement of Tethyan ophiolites in the Eastern Mediterranean and Oman regions. *Earth-Science Reviews* 66, 331-387.

Rowe, M. C., Kent, A. J. R. & Nielsen, R. L. (2009). Subduction influence on oxygen fugacity and trace and volatile elements in basalts across the Cascade volcanic arc. *Journal of Petrology* 50, 61-91.

Rudnick, R. L. & Gao, S. (eds.) (2003). *Composition of the continental crust*: Elsevier

Rutherford, M. J. & Devine, J. D. (2003). Magmatic conditions and magma ascent as indicated by hornblende phase equilibria and reactions in the 1995-2002 Soufrière Hills magma. *Journal of Petrology* 44, 1433-1454.

Sachpazi, M., Galvé, A., Laigle, M., Hirn, A., Sokos, E., Serpetsidaki, A., Marthelot, J.-M., Pi Alperin, J. M., Zelt, B. & Taylor, B. (2007). Moho topography under central Greece and its compensation by Pn time-terms for the accurate location of hypocenters: The example of the Gulf of Corinth 1995 Aigion earthquake. *Tectonophysics* 440, 53-65.

Schulz, B., Klemd, R. & Brätz, H. (2006). Host rock compositional controls on zircon trace- element signatures in metabasites from the Austroalpine basement. *Geochimica et Cosmochimica Acta* 70, 697-710.

Seymour, K. S. & Lalonde, A. (1991). Monitoring oxygen fugacity conditions in pre-, syn- and postcaldera magma chamber of Nisyros volcano, Aegean island arc, Greece. *Journal of Volcanology and Geothermal Research* 46, 231-240.

Sisson, T. W. & Grove, T. L. (1993). Experimental investigations of the role of H2O in calc-alkaline differentiation and subduction zone magmatism. *Contributions to Mineralogy and Petrology* 113, 143-166.

Smith, D. J. (2014). Clinopyroxene precursors to amphibole sponge in arc crust. *Nature Communications* 5, 4329.

Spencer, K. J. & Lindsley, D. H. (1981). A solution model for coexisting iron-titanium oxides. *American Mineralogist* 66, 1189-1201.

Speranza, F., Minelli, L., Pignatelli, A. & Chiappini, M. (2012). The Ionian Sea: The oldest in situ ocean fragment of the world? *Journal of Geophysical Research* 117.

Stouraiti, C., P., M., Tarney, J., Barreiro, B., McGrath, A. M. & Baltatzis, E. (2010). Geochemistry and petrogenesis of late Miocene granitoids, Cyclades, southern Aegean: Nature of source components. *Lithos* 114, 337-352.

Streck, M. J. & Leeman, W. P. (2018). Petrology of "Mt. Shasta" high-magnesian andesite (HMA): A product of multi-stage crustal assembly. *American Mineralogist* 103, 216-240.

Streck, M. J., Leeman, W. P. & Cheesley, J. (2007). High-magnesian andesite from Mount Shasta: A product of magma mixing and contamination, not a primitive mantle melt. *Geology* 35, 351-354.

Tiepolo, M., Tribuzio, R. & Langone, A. (2011). High-Mg andesite petrogenesis by amphibole crystallization and ultramafic crust assimilation: Evidence from Adamello hornblendites (Central Alps, Italy) *Journal of Petrology* 52, 1011-1045.

Tiepolo, M., Vannucci, R., Oberti, R., Foley, S., Bottazzi, P. & Zanetti, A. (2000). Nb and Ta incorporation and fractionation in titanian pargasite and kaersutite: crystal-chemical constraints and implications for natural systems. *Earth and Planetary Science Letters* 176, 185-201.

Tirel, C., Gueydan, F., Tiberi, C. & Brun, J.-P. (2004). Aegean crustal thickness inferred from gravity inversion. Geodynamical implications. *Earth and Planetary Science Letters* 228, 267-280.

Todt, W., Cliff, R. A., Hanser, A. & Hofmann, A. W. (1996). Evaluation of a ^{202}Pb-^{205}Pb double spike for high-precision lead isotope analysis. *Am. Geophys. Un. Geophys. Monograph* 95, 429-437.

Tsuchiyama, A. (1985). Dissolution kinetics of plagioclase in the melt of the system diopside-albite-anorthite, and origin of dusty plagioclase in andesites. *Contributions to Mineralogy and Petrology* 89, 1-16.

White, W. M. & Patchett, J. (1984). Hf-Nd-Sr isotopes and incompatible element abundances in island arcs: implications for magma origins and crust-mantle evolution. *Earth and Planetary Science Letters* 67, 167-185.

Woelki, D., Haase, K. M., Schoenhofen, M. V., Beier, C., Regelous, M., Krumm, S. H. & Günther, T. (2018). Evidence for melting of subducting carbonate-rich sediments in the western Aegean Arc. *Chemical Geology* 483, 463-473.

Wörner, G., Moorbath, S. & Harmon, R. S. (1992). Andean Cenozoic volcanic centers reflect basement isotopic domains. *Geology* 20, 1103-1106.

Zellmer, G. & Turner, S. (2007). Arc dacite genesis pathways: evidence from mafic enclaves and their hosts in Aegean lavas. *Lithos* 95, 346-362.

FIGURE CAPTIONS

Figure 1. (a) Overview map of the Aegean arc showing the volcanic centres with Methana in the west. Benioff zone depths are from Bailey *et al.* (2009). (b) Geologic map of Methana Peninsula modified after Pe-Piper and Piper (2013) showing the lava units and sampling locations.

Figure 2. Selected plagioclase crystals from Methana lavas and profiles of An-contents calculated based on electron microprobe data. (a) Normal zoning with decreasing An-contents from core to rim; (b) Inverse-zonation with increasing An-contents from core to rim; (c) Little zoned plagioclase showing slightly increasing An-contents towards the corroded rim, and (d) sieve-textured plagioclase.

Figure 3. Variations of (a) An contents in plagioclase, **(b) abundance of An-contents in the analysed plagioclase crystals based on a total of 776 analyses, (c)** Mg# in amphibole, and (d) Mg# of clinopyroxene from different lava and enclave samples. Note that most samples show large and continuous variations of the mineral compositions **and that there is no bimodal distribution of An compositions.**

Figure 4. Selected amphibole crystals from Methana lavas along with profiles of Al_2O_3 contents. (a) Euhedral and normally zoned amphibole with high Al_2O_3 contents in the core; (b) oscillatory zoned amphibole; (c) anhedral amphibole with lower Al_2O_3 contents.

Figure 5. (a) Contents of CaO in olivine crystals from Methana compared to those of MORB, and Santorini (Andújar *et al.*, 2015, Huijsmans, 1985, Nicholls, 1971), as well as lavas from Shiveluch and Klyuchevskoy volcanoes in Kamchatka (Gavrilenko *et al.*, 2016). (b) Variations of Cr_2O_3 contents with Mg# in clinopyroxenes from Methana compared to experimentally derived clinopyroxenes **from calc-alkaline basalts to andesites** (Sisson & Grove, 1993). (c) The Al_2O_3 contents versus Mg# of amphiboles from the Methana lavas and enclaves compared

to amphibole from Nisyros cumulate xenoliths (Klaver *et al.*, 2017), and to experimentally derived amphiboles from calc-alkaline melts at 0.9 and 0.7 GPa (Blatter *et al.*, 2013) and 0.4 and 0.2 GPa (Andújar *et al.*, 2015, Cadoux *et al.*, 2014). The MgO contents in the legend are those of the host rocks. **(d) Variation of the FeO versus An contents in plagioclase crystals from the Methana lavas and enclaves compared to those from Nisyros cumulate xenoliths (Klaver *et al.*, 2017).**

Figure 6. (a) The Eu anomaly ($Eu/Eu^* = Eu_N/((Sm_N+Gd_N)/2)$ versus the chondrite-normalized $(La/Sm)_N$ ratios of amphiboles from Methana enclaves and lavas in comparison to amphibole from Nisyros cumulate xenoliths (Klaver *et al.*, 2017), from the calc-alkaline Adamello intrusion in the Alps (Tiepolo *et al.*, 2011), and lavas from Savo volcano in the Solomon island arc (Smith, 2014). (b) The Nb/La ratios of amphibole versus the chondrite-normalized La/Sm ratios of amphiboles from Methana enclaves and lavas in comparison to other amphibole compositions.

Figure 7. The fO_2 and temperatures of lavas calculated from ilmenite-magnetite pairs (Lepage, 2003, Spencer & Lindsley, 1981) in different samples from Methana lavas and enclaves compared to data from Santorini and Nisyros (Barton & Huijsmans, 1986, Cottrell *et al.*, 1999, Fabbro *et al.*, 2013, Seymour & Lalonde, 1991).

Figure 8. Major element contents plotted versus SiO_2 concentrations for lavas and enclaves from Methana in comparison to volcanic rocks from Santorini and Nisyros (Bailey *et al.*, 2009, Braschi *et al.*, 2012, Buettner *et al.*, 2005, Elburg *et al.*, 2018, Francalanci *et al.*, 1995, Innocenti *et al.*, 1981, Kirchenbaur *et al.*, 2011, Klaver *et al.*, 2017, Nicholls, 1971). The classification in (a) is after Le Maitre *et al.* (1989) and shows that Methana magmas resemble those from Santorini and Nisyros. The TiO_2 and FeO^T contents of Santorini lavas show different trends to those of Methana and Nisyros. 8f shows a mixing line between basaltic andesite and dacite magma with the crosses showing 10% increments.

Figure 9. Variations of (a) Ni versus SiO_2, (b) Sc versus SiO_2, (c) Sr versus SiO_2 and (d) Zr versus SiO_2 for the lavas and enclaves of Methana in comparison to those from Santorini and Nisyros. Data sources as in Figure 8.

Figure 10. Variations of (a) chondrite-normalized $(La/Sm)_N$ versus SiO_2, (b) Nb/Zr versus SiO_2, (c) Ba/Th versus SiO_2, (d) $^{143}Nd/^{144}Nd$ versus SiO_2, (e) Eu/Eu* versus SiO_2, and (f) Th/Nd versus SiO_2, comparing the Methana lavas and enclaves to volcanic rocks from Santorini and Nisyros. Data sources as in Figure 8 and Martinique data are from Labanieh *et al.* (2012). Also shown is the range of compositions of depleted mid-ocean ridge basalts (N-MORB (Hofmann, 1988)).

Figure 11. Variation of (a) $^{143}Nd/^{144}Nd$ versus $^{87}Sr/^{86}Sr$, (b) $^{143}Nd/^{144}Nd$ versus $^{206}Pb/^{204}Pb$ and (c) $^{208}Pb/^{204}Pb$ versus $^{206}Pb/^{204}Pb$ for the Methana lavas and enclaves and rocks from Santorini and Nisyros as well as sediments from the Hellenic Trench and Aegean granites. Model curves show (1) mixing between the mantle wedge and subducted sediment, and (2) assimilation-fractional crystallisation curves are based on the model of Bohrson and Spera (2003). Data sources as in Figure 8 and Methana enclaves are from Woelki *et al.* (2018). Also shown are compositions of sediments from the eastern Mediterranean (Klaver *et al.*, 2015) and Aegean granitoids (Altherr & Siebel, 2002, Juteau *et al.*, 1986, Stouraiti *et al.*, 2010).

Figure 12. (a) Variation of $^{143}Nd/^{144}Nd$ versus $(La/Sm)_N$ and (b) $^{143}Nd/^{144}Nd$ versus Th/Nd for the Methana lavas and enclaves in comparison to lavas from Santorini and Nisyros as well as to Neogene sediments and Aegean granites. The model curves in (b) indicate the mantle-sediment mixing and the EC-RAFC model for the Methana magmas with the first number indicating the mass fractionated and the second the mass assimilated. Note that the variation of the enclaves and many of the lavas indicate little assimilation (<2%) but up to 34% fractional crystallisation whereas the most extreme lava compositions require significant assimilation. Data sources as in Figures 8 and 11.

SUPPLEMENTAL MATERIAL

Supplemental Table 1: Whole rock major element, trace element and radiogenic isotope data of the lavas and mineral major element data of the Methana lavas. Thermobarometric calculations were determined using methods described in the main text. Samples marked in bold were predominantly published by Woelki *et al.* (2018).

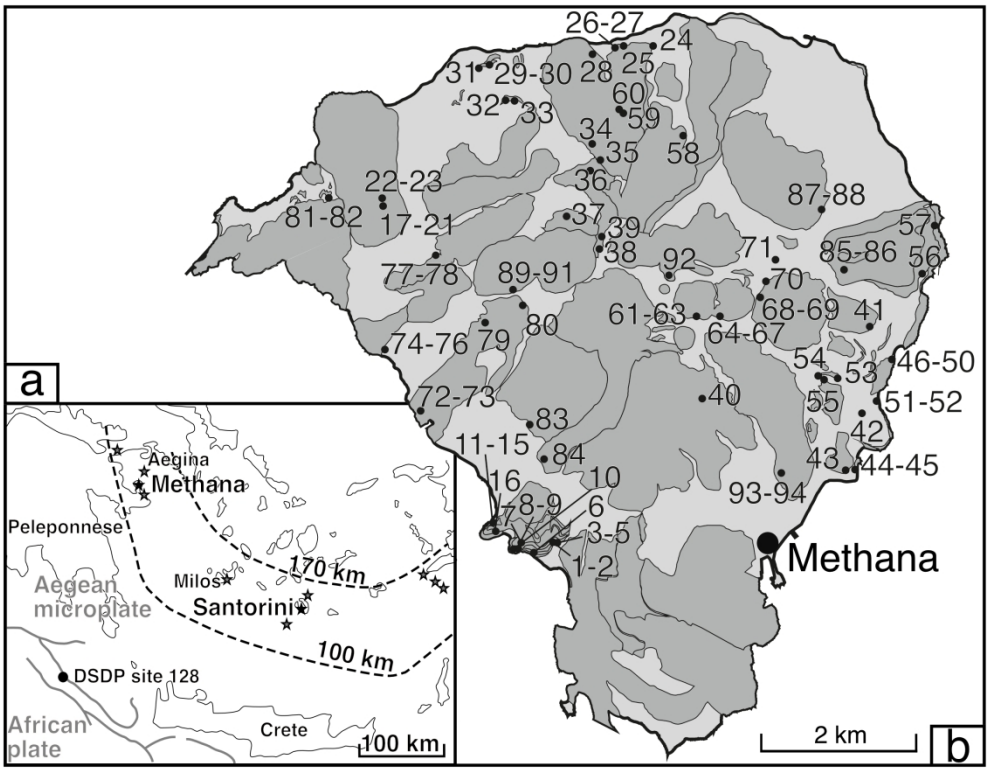

Figure 1. (a) Overview map of the Aegean arc showing the volcanic centres with Methana in the west. Benioff zone depths are from Bailey et al. (2009). (b) Geologic map of Methana Peninsula modified after Pe-Piper and Piper (2013) showing the lava units and sampling locations.

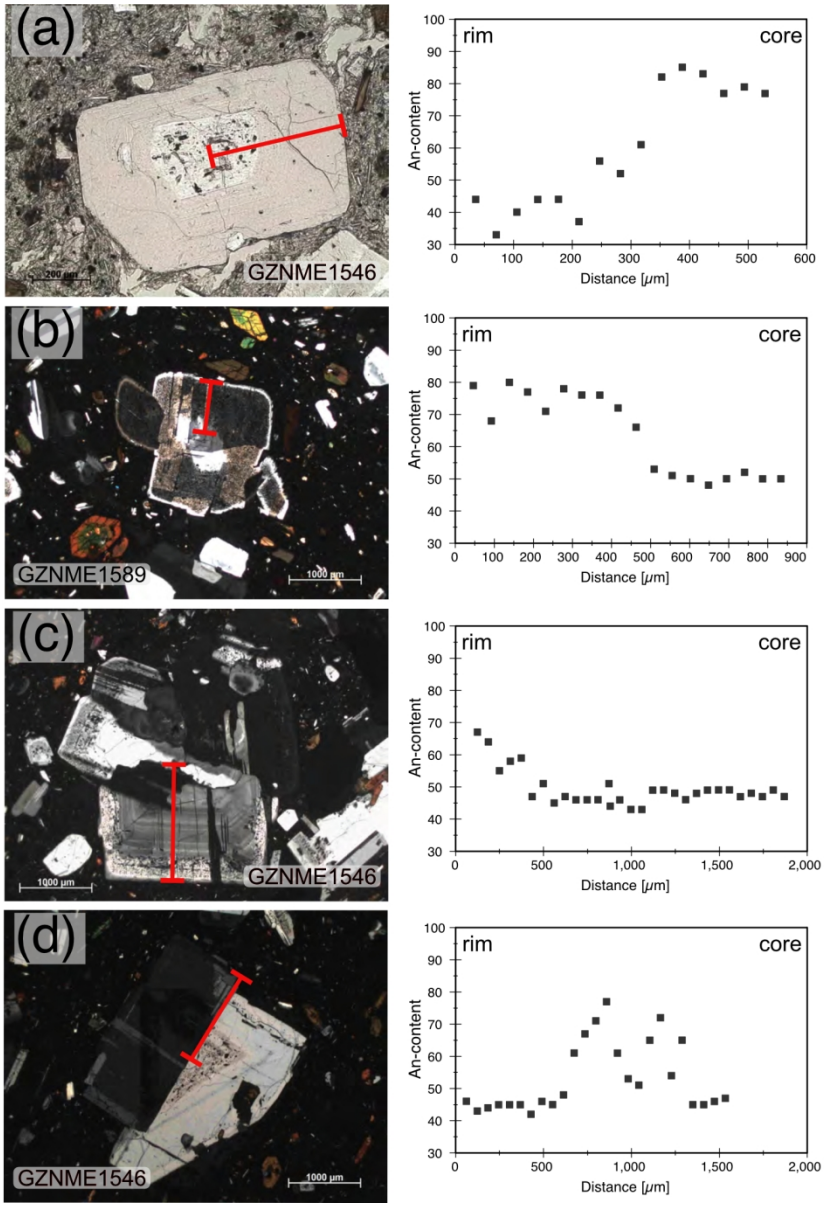

Figure 2. Selected plagioclase crystals from Methana lavas and profiles of An-contents calculated based on electron microprobe data. (a) Normal zoning with decreasing An-contents from core to rim; (b) Inverse-zonation with increasing An-contents from core to rim; (c) Little zoned plagioclase showing slightly increasing An-contents towards the corroded rim, and (d) sieve-textured plagioclase.

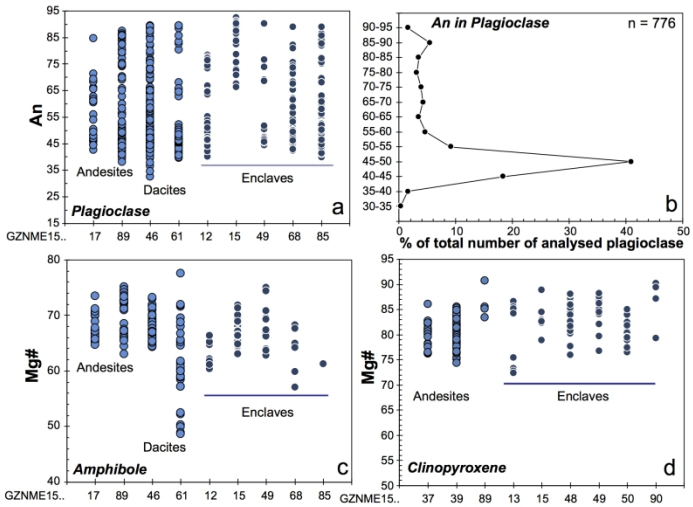

Figure 3. Variations of (a) An contents in plagioclase, (b) abundance of An-contents in the analysed plagioclase crystals based on a total of 776 analyses, (c) Mg# in amphibole, and (d) Mg# of clinopyroxene from different lava and enclave samples. Note that most samples show large and continuous variations of the mineral compositions and that there is no bimodal distribution of An compositions.

209x296mm (300 x 300 DPI)

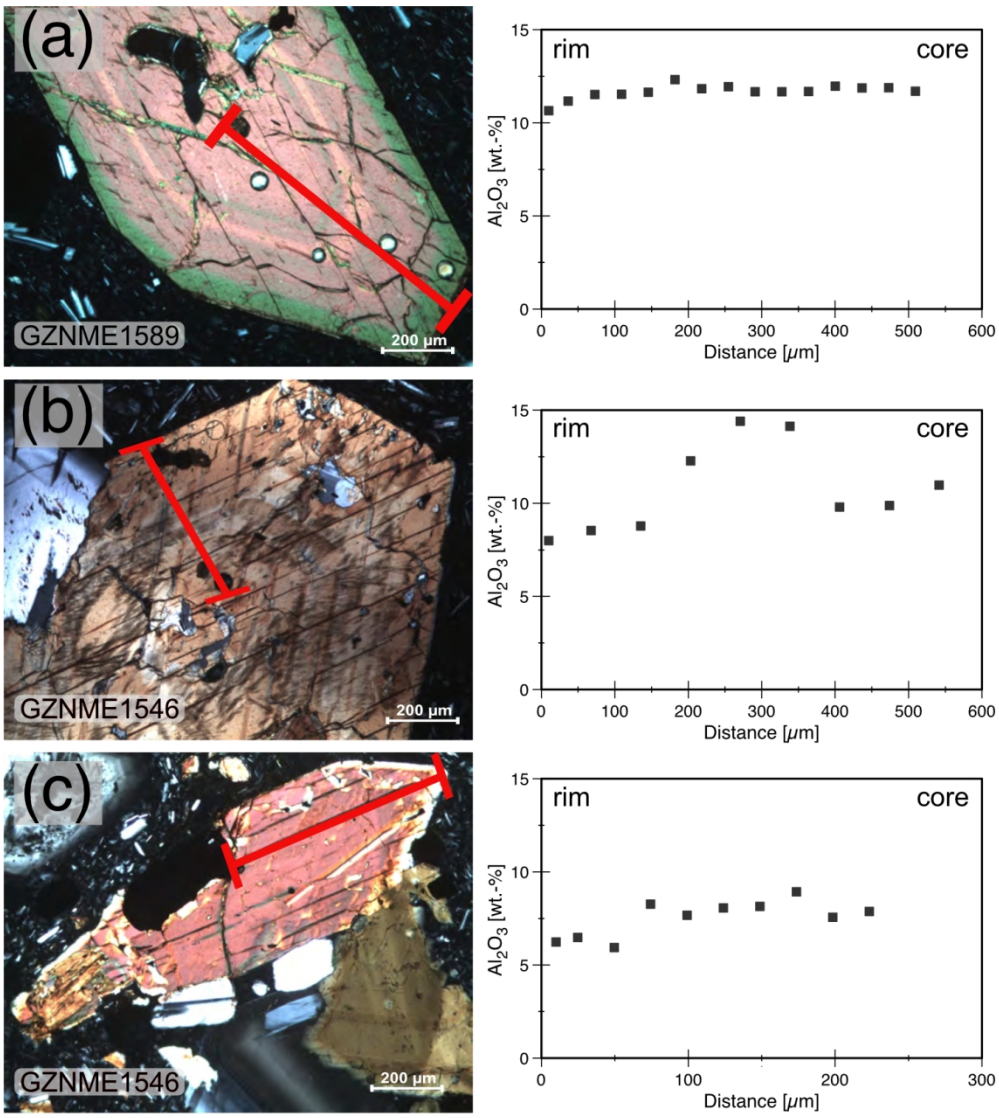

Figure 4. Selected amphibole crystals from Methana lavas along with profiles of Al_2O_3 contents. (a) Euhedral and normally zoned amphibole with high Al_2O_3 contents in the core; (b) oscillatory zoned amphibole; (c) anhedral amphibole with lower Al_2O_3 contents.

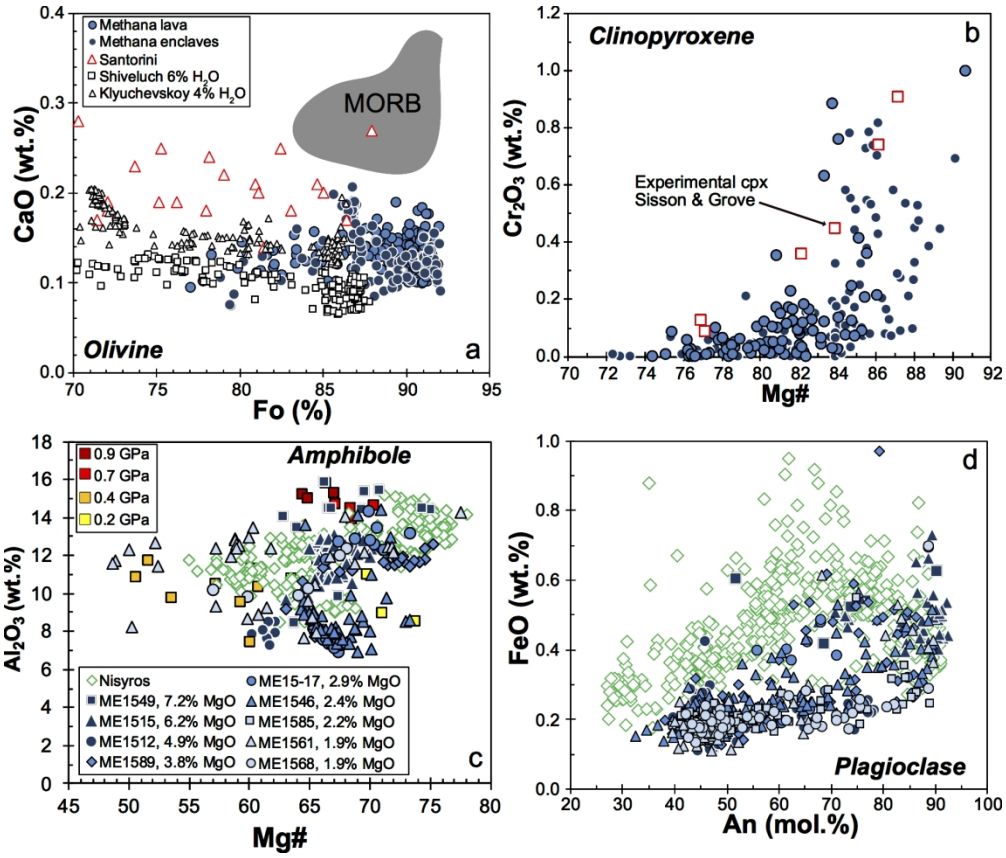

Figure 5. (a) Contents of CaO in olivine crystals from Methana compared to those of MORB, and Santorini (Andújar et al., 2015b, Huijsmans, 1985, Nicholls, 1971), as well as lavas from Shiveluch and Klyuchevskoy volcanoes in Kamchatka (Gavrilenko et al., 2016). (b) Variations of Cr_2O_3 contents with Mg# in clinopyroxenes from Methana compared to experimentally derived clinopyroxenes from calc-alkaline basalts to andesites (Sisson & Grove, 1993). (c) The Al_2O_3 contents versus Mg# of amphiboles from the Methana lavas and enclaves compared to amphibole from Nisyros cumulate xenoliths (Klaver et al., 2017), and to experimentally derived amphiboles from calc-alkaline melts at 0.9 and 0.7 GPa (Blatter et al., 2013) and 0.4 and 0.2 GPa (Andújar et al., 2015, Cadoux et al., 2014). The MgO contents in the legend are those of the host rocks. (d) Variation of the FeO versus An contents in plagioclase crystals from the Methana lavas and enclaves compared to those from Nisyros cumulate xenoliths (Klaver et al., 2017).

162x137mm (300 x 300 DPI)

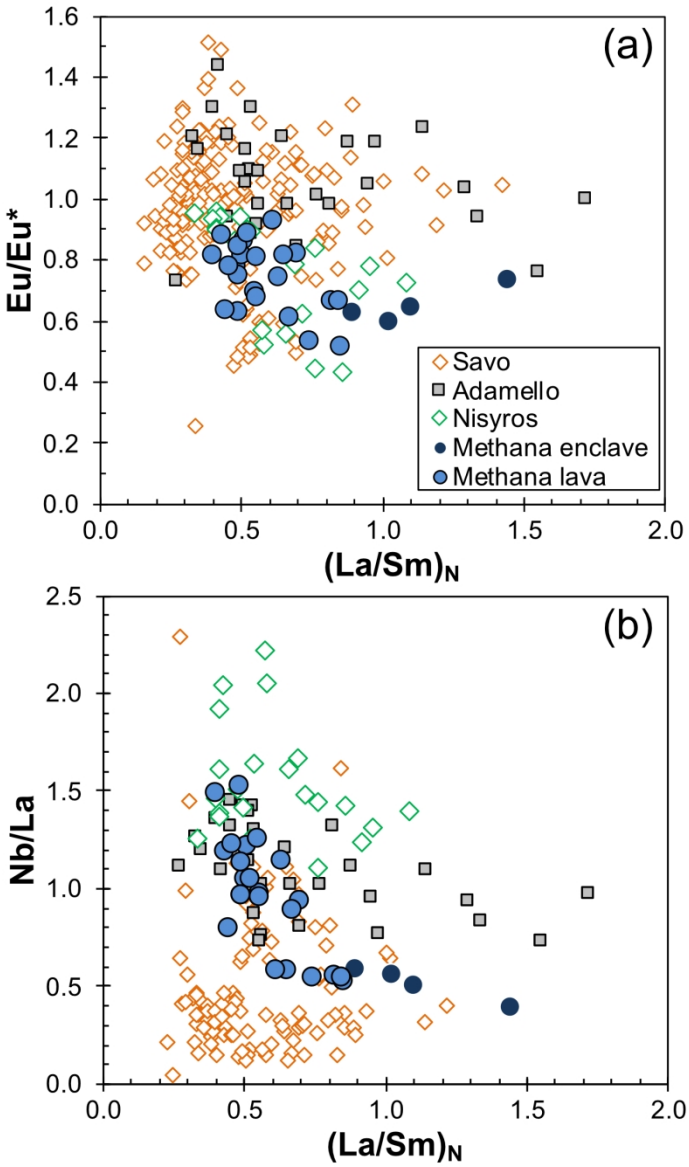

Figure 6. (a) The Eu anomaly ($Eu/Eu^* = Eu_N/((Sm_N+Gd_N)/2)$) versus the chondrite-normalized La/Sm ratios of amphiboles from Methana enclaves and lavas in comparison to amphibole from Nisyros cumulate xenoliths (Klaver et al., 2017), from the calc-alkaline Adamello intrusion in the Alps (Tiepolo et al., 2011), and lavas from Savo volcano in the Solomon island arc (Smith, 2014). (b) The Nb/La ratios of amphibole versus the chondrite-normalized La/Sm ratios of amphiboles from Methana enclaves and lavas in comparison to other amphibole compositions.

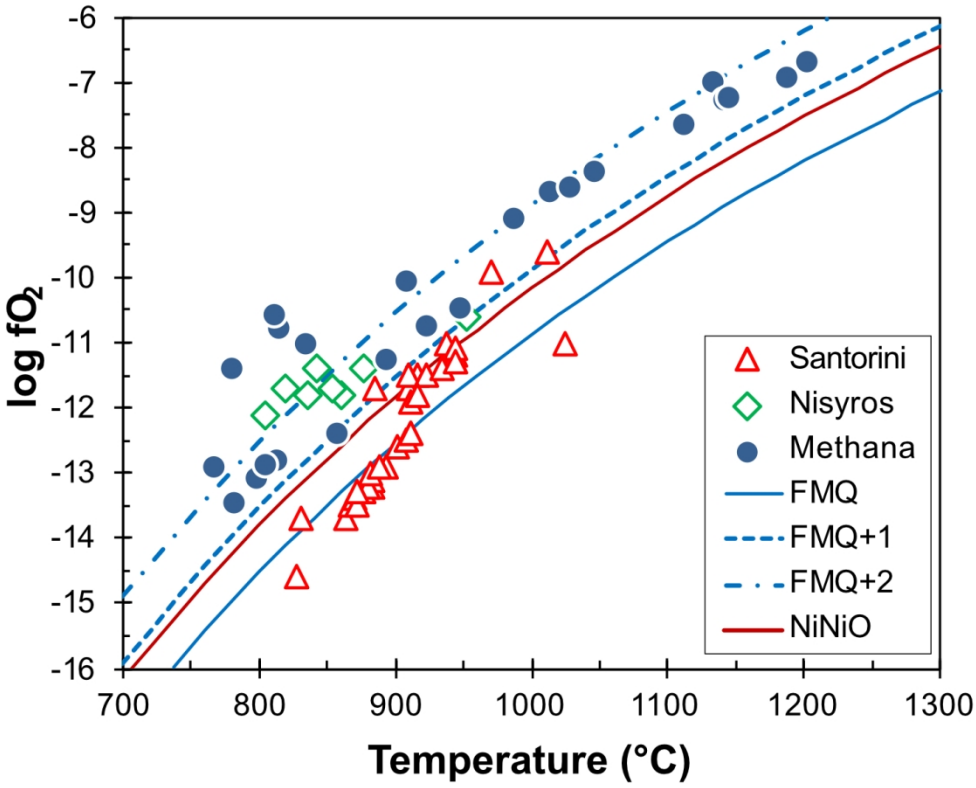

Figure 7. The fO_2 and temperatures of lavas calculated from ilmenite-magnetite pairs (Lepage, 2003, Spencer & Lindsley, 1981) in different samples from Methana lavas and enclaves compared to data from Santorini and Nisyros (Barton & Huijsmans, 1986, Cottrell et al., 1999, Fabbro et al., 2013, Seymour & Lalonde, 1991).

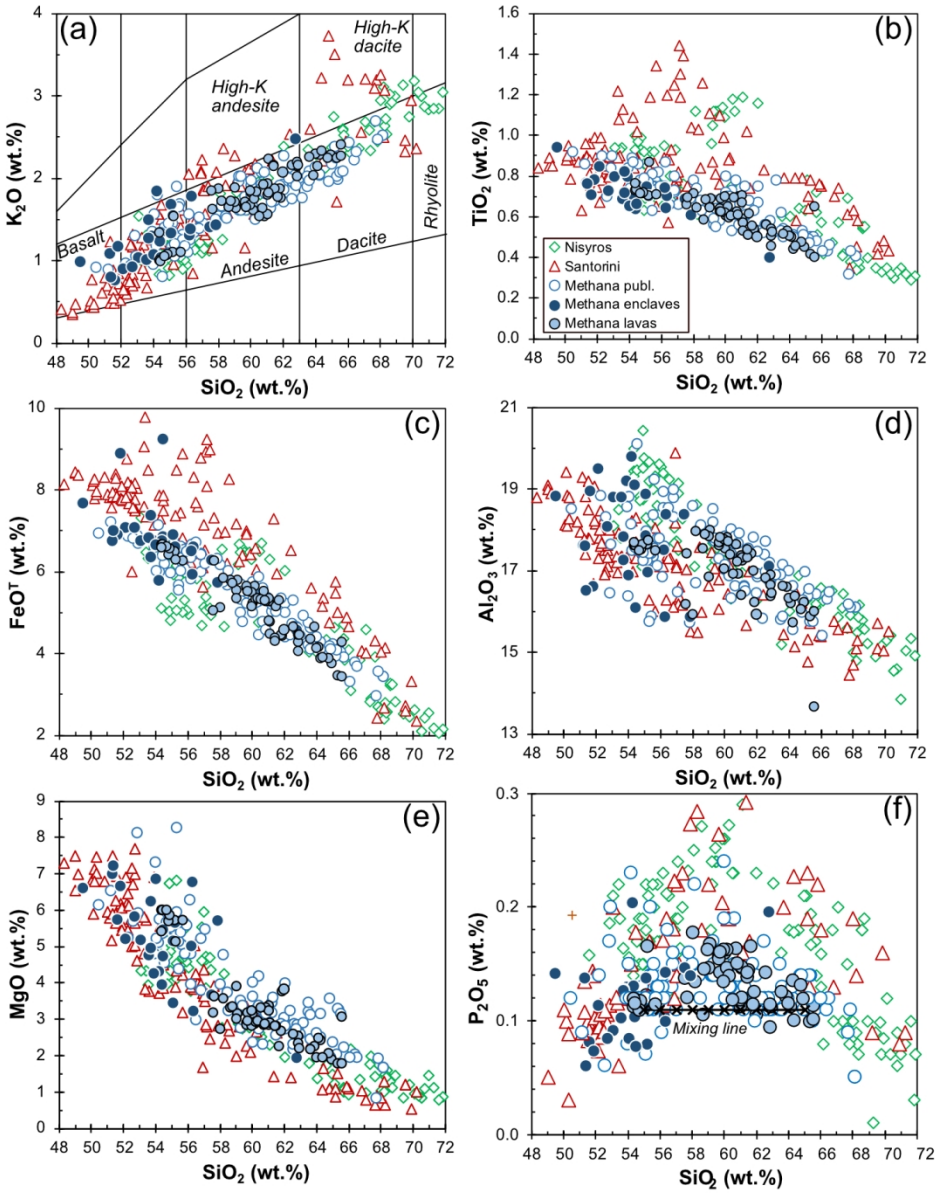

Figure 8. The concentrations of major elements plotted versus SiO2 concentrations for lavas and enclaves from Methana in comparison to volcanic rocks from Santorini and Nisyros (Bailey et al., 2009, Braschi et al., 2012, Buettner et al., 2005, Elburg et al., 2018, Francalanci et al., 1995, Innocenti et al., 1981, Kirchenbaur et al., 2011, Klaver et al., 2017, Nicholls, 1971). The classification in (a) is after Le Maitre et al. (1989) and shows that Methana magmas resemble those from Santorini and Nisyros. The TiO_2 and FeO^T contents of Santorini lavas show different trends to those of Methana and Nisyros. 8f shows a mixing line between basaltic andesite and dacite magma with the crosses showing 10% increments.

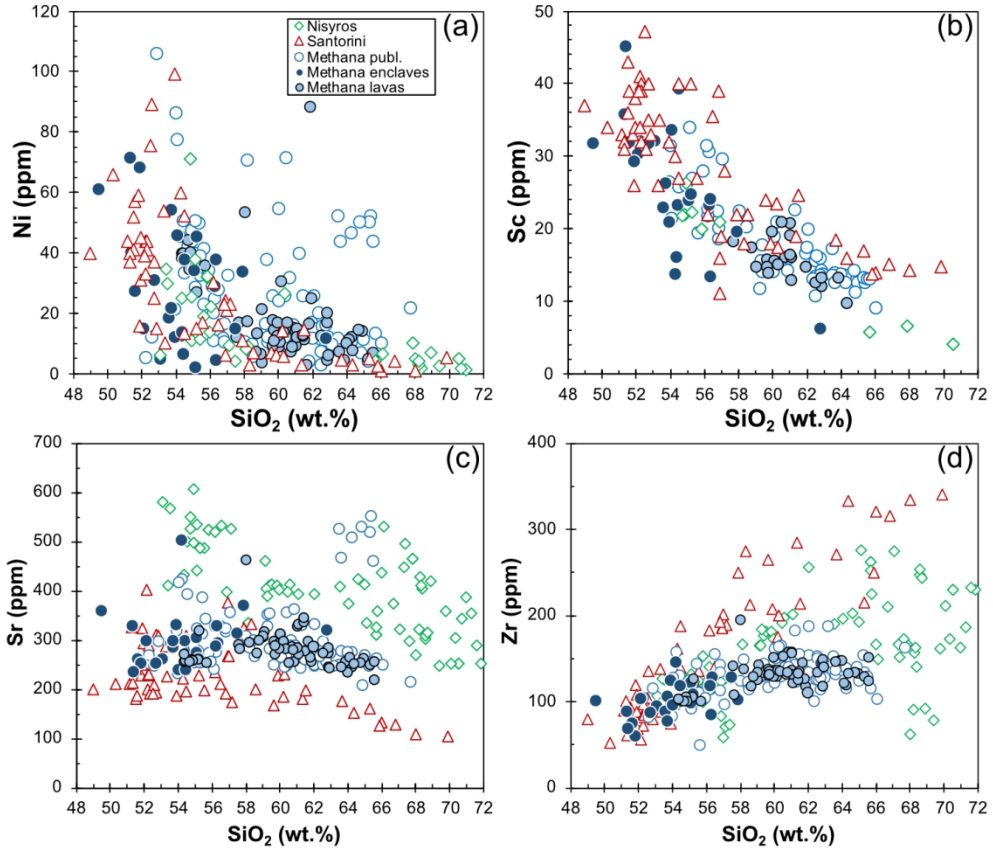

Figure 9. Variations of (a) Ni versus SiO_2, (b) Sc versus SiO_2, (c) Sr versus SiO_2 and (d) Zr versus SiO_2 for the lavas and enclaves of Methana in comparison to those from Santorini and Nisyros. Data sources as in Figure 8.

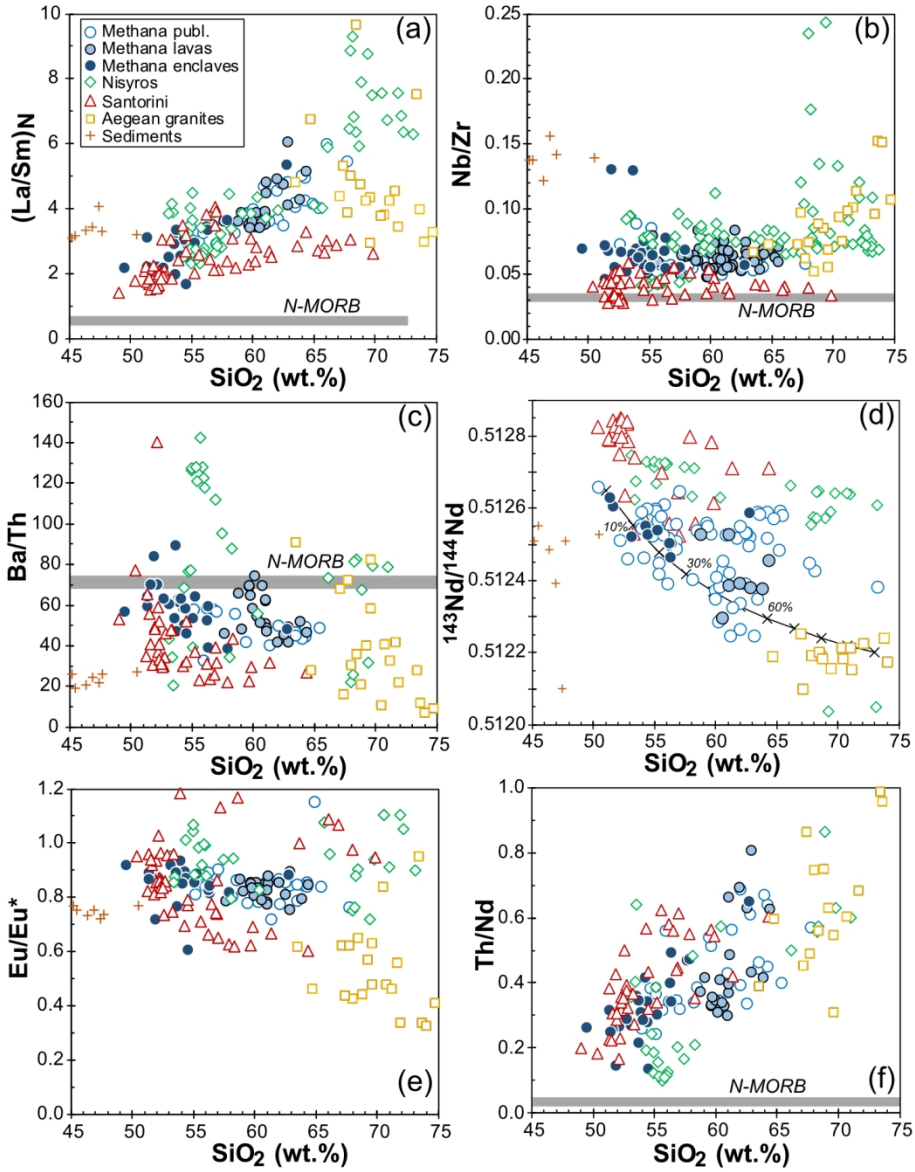

Figure 10. Variations of (a) chondrite-normalized $(La/Sm)_N$ versus SiO_2, (b) Nb/Zr versus SiO_2, (c) Ba/Th versus SiO_2, (d) $^{143}Nd/^{144}Nd$ versus SiO_2, (e) Eu/Eu* versus SiO_2, and (f) Th/Nd versus SiO_2, comparing the Methana lavas and enclaves to volcanic rocks from Santorini and Nisyros. Data sources as in Figure 8 and Martinique data are from Labanieh et al. (2012). Also shown is the range of compositions of depleted mid-ocean ridge basalts (N-MORB (Hofmann, 1988)).

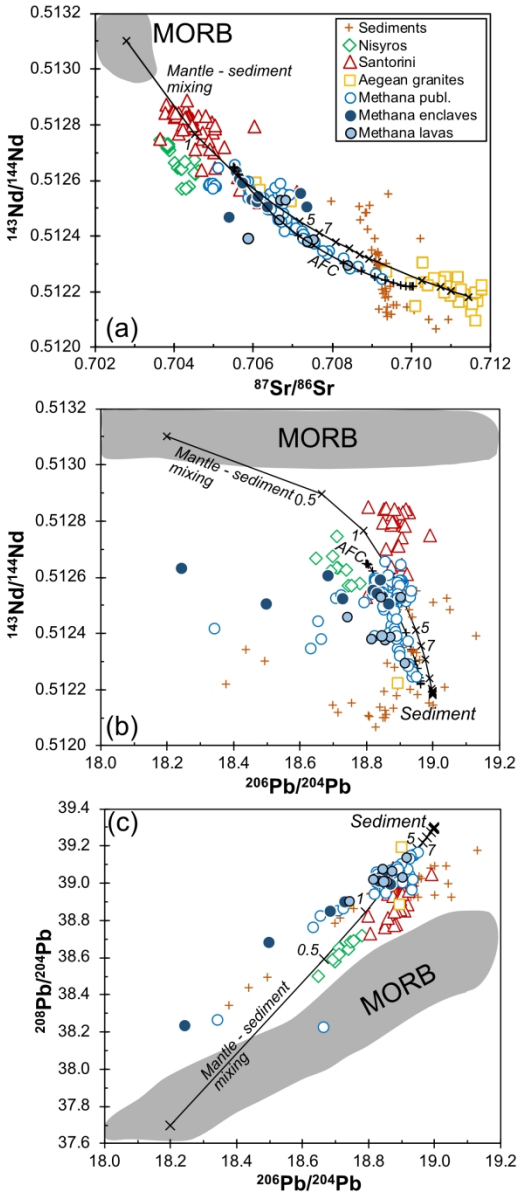

Figure 11. Variation of (a) $^{143}Nd/^{144}Nd$ versus $^{87}Sr/^{86}Sr$, (b) $^{143}Nd/^{144}Nd$ versus $^{206}Pb/^{204}Pb$ and (c) $^{208}Pb/^{204}Pb$ versus $^{206}Pb/^{204}Pb$ for the Methana lavas and enclaves and rocks from Santorini and Nisyros as well as sediments from the Hellenic Trench and Aegean granites. Model curves show (1) mixing between the mantle wedge and subducted sediment, and (2) assimilation-fractional crystallisation curves are based on the model of Bohrson and Spera (2003). Data sources as in Figure 8 and Methana enclaves are from Woelki et al. (2018). Also shown are compositions of sediments from the eastern Mediterranean (Klaver et al., 2015) and Aegean granitoids (Altherr & Siebel, 2002, Juteau et al., 1986, Stouraiti et al., 2010).

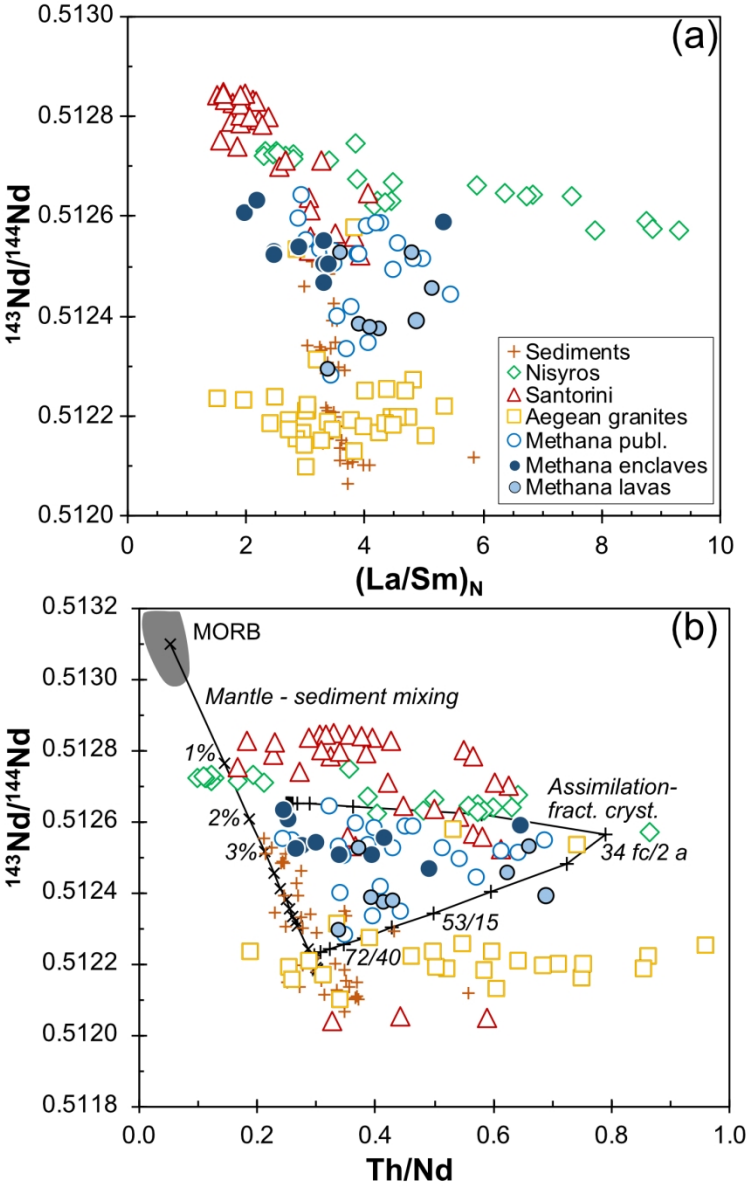

Figure 12. (a) Variation of $^{143}Nd/^{144}Nd$ versus $(La/Sm)_N$ and (b) $^{143}Nd/^{144}Nd$ versus Th/Nd for the Methana lavas and enclaves in comparison to lavas from Santorini and Nisyros as well as to Neogene sediments and Aegean granites. The model curves in (b) indicate the mantle-sediment mixing and the EC-RAFC model for the Methana magmas with the first number indicating the mass fractionated and the second the mass assimilated. Note that the variation of the enclaves and many of the lavas indicate little assimilation (<2%) but up to 34% fractional crystallisation whereas the most extreme lava compositions require significant assimilation. Data sources as in Figures 8 and 11.

Table 1. Major, trace and isotope data of IGSN sample # of Methana whole rock samples. Data with * were measured by XRF. All major element contents are given in wt.-%, trace elements in ppm. Standard measurements for comparison are given in supplementary Table 1.

IEGZN-	ME1501	ME1502	ME1503	ME1504	ME1505	M15E06	ME1509	ME1512	ME1514
Locality	1	1	2	2	2	3	5	7	7
Lat. [N]	37.580	37.580	37.580	37.580	37.580	37.579	37.579	37.582	37.582
Long. [E]	23.357	23.357	23.357	23.357	23.357	23.355	23.352	23.348	23.348
Elevation [m]	22.00	22.00	23.10	23.10	23.10	22.24	23.57	29.18	29.18
SiO_2	55.19	55.71	54.40	54.44	54.81	54.88	54.72	53.72	59.04
TiO_2	0.71	0.71	0.73	0.74	0.71	0.72	0.71	0.82	0.65
Al_2O_3	17.64	17.48	17.60	17.61	17.51	17.64	17.48	17.82	16.84
Fe_2O_3	7.21	6.96	7.39	7.41	7.12	7.30	7.34	8.18	6.17
MnO	0.14	0.14	0.14	0.15	0.14	0.14	0.14	0.21	0.13
MgO	5.71	5.71	6.01	5.99	5.70	5.85	6.01	4.95	3.90
CaO	9.08	8.96	9.38	9.55	9.57	9.26	9.38	8.21	7.10
Na_2O	2.93	2.96	2.95	2.82	2.95	2.79	2.85	3.81	3.18
K_2O	1.10	1.10	1.00	0.99	1.06	1.08	1.05	1.49	1.88
P_2O_5	0.12	0.11	0.11	0.12	0.12	0.11	0.11	0.13	0.15
LOI	0.00	0.00	0.11	0.02	0.15	0.08	0.04	0.51	0.78
Total	99.83	99.84	99.83	99.82	99.84	99.84	99.83	99.83	99.82
Li								16.0	
Sc								26.1	
V								144	
V*	166	172	195	199	186	195	192	158	132
Cr								57.8	
Cr*	138	128	145	150	132	138	145	71.7	84.3
Co								17.2	
Ni								21.8	
Ni*	36.5	35.4	39.5	39.6	34.4	40.0	43.9	21.4	21.3
Cu								16.3	
Zn								82.6	
Zn*	61.9	61.5	61.3	69.4	60.2	60.1	61.8	91.4	59.9
Ga								29.2	
Ga*	13.8	17.5	17.9	15.7	15.0	14.8	15.7	15.5	17.3
Rb								48.4	
Rb*	32.8	33.2	29.7	31.0	32.1	32.6	32.0	52.1	60.4
Sr								270	
Sr*	259	253	256	258	261	258	256	283	305
Y								33.7	
Y*	18.9	19.2	21.6	22.6	19.3	21.4	22.9	34.3	23.4
Zr								20.1	
Zr*	105	100	103	101	105	99.8	99.7	76.6	124.6

IEGZN-	ME1501	ME1502	ME1503	ME1504	ME1505	M15E06	ME1509	ME1512	ME1514
Nb								11.6	
Nb*	6.60	5.90	6.50	6.70	5.30	5.30	6.70	9.90	10.40
Mo								0.98	
Sn								1.92	
Cs								1.55	
Ba								409	
Ba*	245	234	250	229	253	229	237	410	401
La								16.5	
Ce								37.8	
Pr								4.98	
Nd								21.4	
Sm								5.40	
Eu								1.37	
Gd								5.39	
Tb								0.89	
Dy								5.73	
Ho								1.17	
Er								3.40	
Tm								0.51	
Yb								3.36	
Lu								0.49	
Hf								1.07	
Ta								0.66	
W								0.59	
Tl								0.33	
Pb								8.11	
Th								4.60	
Th*	3.60	5.60	7.90	4.30	3.60	4.30	5.20	3.60	8.90
U								1.36	
^{143}Nd/^{144}Nd									
^{87}Sr/^{86}Sr									
^{206}Pb/^{204}Pb									
^{207}Pb/^{204}Pb									
^{208}Pb/^{204}Pb									

IEGZN-	ME1516	ME1519	ME1520	ME1522	ME1523	ME1524	ME1526	ME1527	ME1528
Locality	8	9	9	10	10	11	13	13	14
Lat. [N]	37.581	37.619	37.619	37.619	37.619	37.637	37.637	37.637	37.637
Long. [E]	23.348	23.333	23.333	23.333	23.333	23.372	23.366	23.366	23.363
Elevation [m]	35.14	402.58	402.58	383.82	383.82	26.98	62.74	62.74	48.01
SiO_2	55.25	61.45	61.43	62.79	65.57	60.07	60.86	61.03	60.75
TiO_2	0.87	0.51	0.51	0.40	0.65	0.60	0.70	0.71	0.63
Al_2O_3	17.73	17.32	17.52	17.09	13.65	17.53	16.91	17.31	17.63
Fe_2O_3	7.00	4.85	4.78	5.06	4.75	5.81	5.84	5.94	6.13
MnO	0.14	0.11	0.11	0.12	0.12	0.13	0.12	0.12	0.13
MgO	5.12	2.81	2.81	1.92	3.05	3.15	3.31	3.24	2.84
CaO	8.92	6.12	6.18	5.28	4.30	6.68	7.11	6.41	6.51
Na_2O	3.09	3.71	3.76	3.84	3.48	3.38	3.35	2.82	3.44
K_2O	1.54	2.16	2.14	2.47	2.40	1.82	1.54	1.56	1.63
P_2O_5	0.17	0.14	0.14	0.20	0.11	0.16	0.11	0.11	0.16
LOI	0.00	0.65	0.45	0.67	1.75	0.51	0.00	0.58	0.00
Total	99.82	99.83	99.83	99.83	99.83	99.83	99.85	99.83	99.85
Li				33.0				22.5	15.2
Sc				6.06				20.6	15.9
V				55.6				122	138
V*	173	95.9	97.6	67.4	86.4	121	137	122	120
Cr				9.62				51.1	10.0
Cr*	112	33.0	24.5	16.1	29.8	32.2	65.1	61.9	18.3
Co				8.36				13.8	15.0
Ni				5.74				10.34	7.37
Ni*	26.8	12.2	12.8	11.7	6.70	8.80	15.0	13.9	7.10
Cu				11.2				9.75	13.0
Zn				61.7				57.9	64.1
Zn*	57.9	50.3	49.3	66.9	49.8	61.6	61.5	63.4	66.5
Ga				30.9				37.15	42.9
Ga*	15.4	14.2	16.9	19.8	20.9	17.3	16.9	18.5	14.6
Rb				82.1				44.9	49.5
Rb*	45.6	84.8	84.0	85.4	95.3	60.6	47.3	45.4	46.4
Sr				303				279	311
Sr*	320	337	346	319	220	311	255	278	286
Y				15.8				22.2	19.8
Y*	22.9	16.8	15.0	14.9	17.2	21.4	24.5	24.5	21.7
Zr				151				112	120
Zr*	127	125	132	144	151	136	157	157	131
Nb				7.54				9.10	6.93
Nb*	10.0	8.40	7.30	8.10	8.90	9.00	9.60	9.00	7.20
Mo				1.64				0.83	0.84

IEGZN-	ME1516	ME1519	ME1520	ME1522	ME1523	ME1524	ME1526	ME1527	ME1528
Sn				1.34				0.97	1.17
Cs				4.69				0.92	1.06
Ba				457				386	430
Ba*	340	454	445	478	524	420	329	353	399
La				22.9				23.2	21.0
Ce				39.6				45.4	42.2
Pr				4.15				5.34	4.81
Nd				14.7				20.8	18.8
Sm				2.76				4.27	3.79
Eu				0.77				1.08	1.04
Gd				2.42				4.11	3.59
Tb				0.39				0.65	0.56
Dy				2.47				4.10	3.51
Ho				0.51				0.83	0.72
Er				1.55				2.45	2.17
Tm				0.25				0.35	0.32
Yb				1.73				2.34	2.22
Lu				0.28				0.35	0.34
Hf				3.73				3.32	3.13
Ta				0.62				0.63	0.45
W				1.14				0.60	0.56
Tl				0.50				0.12	0.21
Pb				16.4				7.62	7.72
Th				9.56				6.23	6.18
Th*	5.30	10.9	11.0	10.9	13.1	11.8	7.00	7.70	6.40
U				2.45				1.21	1.38
^{143}Nd/^{144}Nd				0.51259					
^{87}Sr/^{86}Sr				0.70576					
^{206}Pb/^{204}Pb				18.84					
^{207}Pb/^{204}Pb				15.69					
^{208}Pb/^{204}Pb				39.04					

IEGZN-	ME1529	ME1530.2	ME1532	ME1533	ME1534	ME1535	ME1536	ME1537	ME1538
Locality	15	15	17	18	19	20	21	22	23
Lat. [N]	37.635	37.635	37.631	37.631	37.626	37.624	37.623	37.617	37.614
Long. [E]	23.347	23.347	23.350	23.352	23.363	23.364	23.362	23.359	23.365
Elevation [m]	60.34	60.34	182.52	203.18	307.18	350.53	367.78	475.99	535.79
SiO_2	63.88	54.53	85.76	62.88	59.69	60.15	59.74	61.12	59.76
TiO_2	0.53	0.66	0.30	0.50	0.64	0.65	0.69	0.57	0.62
Al_2O_3	16.60	16.06	6.09	16.90	17.61	17.80	17.69	17.23	17.80
Fe_2O_3	5.18	10.25	1.59	4.75	6.21	6.28	6.12	5.29	6.13
MnO	0.12	0.26	0.03	0.11	0.13	0.13	0.13	0.12	0.13
MgO	2.25	5.45	0.99	2.53	2.88	2.88	3.16	2.88	2.95
CaO	5.65	8.41	0.32	6.13	6.69	6.70	7.01	6.73	6.67
Na_2O	3.49	3.09	0.73	3.60	3.71	3.48	3.20	3.31	3.42
K_2O	2.03	1.03	2.08	2.02	1.69	1.61	1.65	1.83	1.65
P_2O_5	0.12	0.08	0.01	0.09	0.16	0.16	0.14	0.12	0.16
LOI	0.00	0.00	2.03	0.33	0.44	0.00	0.32	0.65	0.55
Total	99.85	99.81	99.92	99.84	99.84	99.84	99.85	99.85	99.84
Li	25.2	26.1			17.0	12.6		22.0	17.7
Sc	13.2	39.2			15.7	15.4		15.9	13.8
V	86.6	175			134	134		128	107
V*	78.5	183	54.3	79.4	127	129	75.3	118	119
Cr	16.7	160			12.2	11.3		27.2	21.0
Cr*	23.4	174	47.2	37.0	15.2	14.8	48.5	36.9	21.6
Co	10.0	20.7			14.6	15.0		14.5	13.1
Ni	5.87	32.1			7.95	7.98		13.7	15.4
Ni*	4.40	37.8	22.8	16.9	9.20	10.3	14.3	14.8	10.8
Cu	9.57	28.9			7.81	13.7		24.0	8.63
Zn	56.9	105			62.5	65.9		50.4	61.6
Zn*	61.2	107	26.0	49.8	68.3	73.0	72.2	55.3	68.0
Ga	43.4	23.6			40.2	42.0		38.9	26.4
Ga*	15.4	17.6	8.10	17.0	16.8	18.6	16.7	15.9	16.8
Rb	68.2	26.0			47.4	47.6		63.4	44.6
Rb*	66.3	27.2	69.9	70.5	47.7	44.9	51.7	61.1	46.8
Sr	271	236			300	312		282	277
Sr*	256	239	34.8	273	294	295	272	272	288
Y	19.0	54.2			18.9	19.6		17.5	19.8
Y*	22.6	54.7	8.50	16.1	23.2	20.6	22.1	19.2	20.9
Zr	30.0	36.4			132	119		48.6	115
Zr*	148	118	57.4	117	137	128	135	121	131
Nb	9.13	8.42			6.61	6.84		7.20	6.69
Nb*	8.70	8.80	5.60	8.70	6.50	6.60	10.20	7.40	6.20
Mo	0.98	1.10			1.07	1.12		0.73	2.66

IEGZN-	ME1529	ME1530.2	ME1532	ME1533	ME1534	ME1535	ME1536	ME1537	ME1538
Sn	1.30	3.24			1.09	1.09		0.99	1.28
Cs	1.90	0.86			1.77	1.11		1.60	1.97
Ba	458	223			405	429		396	369
Ba*	375	244	141	418	390	390	344	376	391
La	27.0	22.6			19.6	20.4		22.7	18.5
Ce	53.8	59.1			40.0	41.2		41.3	36.3
Pr	5.75	8.14			4.56	4.78		4.54	4.17
Nd	21.3	35.8			17.8	18.8		16.8	16.2
Sm	4.10	8.78			3.63	3.83		3.27	3.50
Eu	1.04	1.75			1.01	1.06		0.91	0.94
Gd	3.70	8.53			3.46	3.59		3.14	3.27
Tb	0.59	1.40			0.54	0.56		0.50	0.52
Dy	3.51	8.97			3.40	3.50		3.08	3.32
Ho	0.70	1.82			0.69	0.72		0.64	0.67
Er	2.03	5.22			2.11	2.17		1.90	1.98
Tm	0.30	0.78			0.31	0.32		0.29	0.30
Yb	1.96	5.12			2.16	2.23		1.92	2.02
Lu	0.29	0.74			0.33	0.33		0.30	0.30
Hf	1.19	1.73			3.00	3.11		1.64	3.03
Ta	0.66	0.49			0.43	0.44		0.55	0.45
W	0.66	0.69			0.64	0.55		0.65	0.65
Tl	0.26	0.11			0.23	0.19		0.21	0.15
Pb	20.3	5.67			7.93	6.86		9.06	7.10
Th	8.82	4.84			5.88	5.79		8.17	5.73
Th*	10.3	4.00	5.60	11.0	6.20	7.00	8.80	9.40	4.80
U	1.04	1.00			1.33	1.30		1.84	1.24
^{143}Nd/^{144}Nd	0.51237								
^{87}Sr/^{86}Sr	0.70745								
^{206}Pb/^{204}Pb	18.9								
^{207}Pb/^{204}Pb	15.7								
^{208}Pb/^{204}Pb	39.0								

IEGZN-	ME1539	ME1540	ME1541	ME1542	ME1543	ME1544	ME1545	ME1546	ME1547
Locality	24	25	39	40	41	42	42	43	43
Lat. [N]	37.615	37.599	37.605	37.595	37.588	37.588	37.588	37.602	37.602
Long. [E]	23.365	23.379	23.404	23.402	23.400	23.402	23.402	23.407	23.407
Elevation [m]	536.92	487.60	158.40	81.78	73.06	6.59	6.59	8.32	8.32
SiO_2	57.68	62.56	64.16	64.95	64.75	59.09	59.01	64.29	54.41
TiO_2	0.69	0.56	0.50	0.45	0.47	0.69	0.65	0.44	0.63
Al_2O_3	17.40	16.81	16.19	16.21	16.04	17.98	17.84	15.73	19.07
Fe_2O_3	6.95	5.17	4.62	4.17	4.30	6.44	5.92	4.32	7.49
MnO	0.15	0.13	0.12	0.10	0.10	0.14	0.13	0.11	0.16
MgO	3.62	2.58	2.46	1.88	2.07	3.14	3.02	2.43	3.94
CaO	7.84	5.95	5.77	5.21	5.28	7.11	6.67	5.45	9.05
Na_2O	3.22	3.40	3.73	3.51	3.42	3.45	3.73	3.53	2.80
K_2O	1.62	2.16	2.15	2.29	2.24	1.63	1.71	2.28	1.22
P_2O_5	0.12	0.14	0.11	0.12	0.13	0.17	0.16	0.14	0.13
LOI	0.54	0.38	0.04	0.95	1.03	0.00	1.00	1.12	0.94
Total	99.84	99.83	99.84	99.84	99.84	99.83	99.84	99.83	99.85
Li	19.0	25.3				13.7			15.4
Sc	18.2	12.5				14.6			16.0
V	139	96.1				114			147
V*	150	106	103	70.8	77.7	129	119	97.2	157
Cr	27.7	16.8				10.4			8.26
Cr*	39.5	34.1	25.5	38.2	28.4	15.0	13.9	36.4	16.6
Co	18.3	14.3				12.8			16.5
Ni	18.0	8.98				5.22			7.90
Ni*	16.8	12.2	11.2	14.0	14.4	3.40	6.30	12.1	13.6
Cu	28.1	19.9				8.82			9.47
Zn	57.9	66.8				63.1			68.4
Zn*	59.3	70.5	52.8	48.0	52.6	67.6	63.8	50.8	74.1
Ga	25.1	29.3				27.1			23.3
Ga*	16.7	15.9	13.7	14.1	16.4	19.7	16.9	16.2	16.8
Rb	50.7	73.3				48.6			33.6
Rb*	53.3	75.7	71.5	80.7	80.0	50.6	54.2	75.3	35.0
Sr	269	261				307			290
Sr*	282	274	263	263	254	317	308	245	298
Y	22.9	18.8				21.3			20.4
Y*	22.9	19.4	15.8	17.1	16.5	22.8	21.3	16.6	21.1
Zr	77.2	72.7				121			93.0
Zr*	108	134	121	133	134	142	134	119	98.8
Nb	6.99	8.03				8.20			5.52
Nb*	6.90	7.00	7.80	9.10	9.20	9.80	8.00	8.10	6.50

IEGZN-	ME1539	ME1540	ME1541	ME1542	ME1543	ME1544	ME1545	ME1546	ME1547
Mo	1.04	1.25				1.12			1.09
Sn	0.96	0.88				1.04			1.07
Cs	2.66	3.04				2.22			1.83
Ba	328	466				392			236
Ba*	334	490	483	472	469	407	420	499	253
La	19.0	23.8				24.0			15.0
Ce	34.8	42.0				46.7			28.9
Pr	3.95	4.50				5.21			3.44
Nd	15.3	16.3				19.7			13.8
Sm	3.41	3.25				4.02			3.19
Eu	0.91	0.84				1.05			0.92
Gd	3.57	2.99				3.63			3.16
Tb	0.56	0.47				0.57			0.52
Dy	3.62	2.97				3.61			3.36
Ho	0.75	0.61				0.73			0.69
Er	2.14	1.78				2.12			2.03
Tm	0.31	0.27				0.32			0.31
Yb	2.10	1.83				2.16			2.08
Lu	0.31	0.28				0.33			0.31
Hf	2.26	2.17				3.18			2.51
Ta	0.53	0.64				0.55			0.38
W	0.79	0.99				0.75			0.51
Tl	0.19	0.38				0.25			0.19
Pb	7.66	10.2				7.93			5.74
Th	7.13	10.2				8.16			4.70
Th*	7.10	12.0	11.9	12.9	13.2	8.30	7.90	13.3	4.70
U	1.79	2.33				1.73			1.07
^{143}Nd/^{144}Nd									
^{87}Sr/^{86}Sr									
^{206}Pb/^{204}Pb									
^{207}Pb/^{204}Pb									
^{208}Pb/^{204}Pb									

IEGZN-	ME1551	ME1552	ME1553	ME1554	ME1555	ME1556	ME1559	ME1560	ME1561
Locality	44	44	45	46	47	48	51	52	53
Lat. [N]	37.596	37.596	37.599	37.599	37.599	37.611	37.630	37.630	37.606
Long. [E]	23.405	23.405	23.398	23.396	23.397	23.411	23.368	23.367	23.378
Elevation [m]	4.54	4.54	94.28	132.74	135.41	43.00	274.40	278.80	531.03
SiO_2	58.05	61.87	65.32	61.83	65.57	57.56	59.69	59.99	64.03
TiO_2	0.72	0.52	0.42	0.54	0.40	0.66	0.62	0.62	0.50
Al_2O_3	15.92	16.23	15.87	16.99	15.99	16.16	17.69	17.76	16.32
Fe_2O_3	5.70	4.91	3.85	4.95	3.80	5.60	6.27	6.09	4.60
MnO	0.12	0.12	0.10	0.12	0.10	0.12	0.13	0.13	0.11
MgO	2.74	3.77	1.79	2.67	1.76	3.19	2.83	2.80	1.93
CaO	10.06	6.22	4.75	6.22	4.82	8.70	6.67	6.58	5.24
Na_2O	3.90	3.26	4.18	3.43	3.64	2.98	3.43	3.57	3.45
K_2O	1.87	1.75	2.25	1.87	2.27	1.85	1.70	1.67	2.29
P_2O_5	0.18	0.13	0.10	0.11	0.10	0.14	0.15	0.16	0.11
LOI	0.55	1.06	1.24	1.11	1.40	2.91	0.67	0.47	1.26
Total	99.80	99.83	99.86	99.84	99.86	99.84	99.85	99.85	99.85
Li							16.3		
Sc							14.7		
V							129		
V*	109	103	73.4	108	70.8	121	117	106	68.6
Cr							12.5		
Cr*	119	143	23.2	43.1	23.0	38.6	21.5	24.9	19.9
Co							14.1		
Ni							8.45		
Ni*	53.1	88.2	4.70	16.3	5.40	11.9	17.7	12.4	10.0
Cu							16.6		
Zn							62.7		
Zn*	70.9	55.0	49.4	58.3	49.6	55.6	67.3	67.9	60.5
Ga							40.6		
Ga*	16.8	16.0	15.4	13.6	12.8	16.2	17.3	16.0	16.0
Rb							48.0		
Rb*	64.3	58.4	76.3	61.8	77.7	53.6	48.0	46.9	71.7
Sr							310		
Sr*	462	255	249	264	255	291	297	293	235
Y							19.0		
Y*	21.3	17.4	16.4	18.3	16.0	21.2	22.7	23.5	23.0
Zr							122		
Zr*	194	118	128	126	124	141	130	129	148
Nb							6.77		
Nb*	12.2	7.50	8.00	7.10	8.80	6.90	7.10	6.60	7.90

IEGZN-	ME1551	ME1552	ME1553	ME1554	ME1555	ME1556	ME1559	ME1560	ME1561
Mo							1.22		
Sn							1.18		
Cs							1.76		
Ba							412		
Ba*	419	388	491	395	443	379	366	387	434
La							19.8		
Ce							40.4		
Pr							4.56		
Nd							17.8		
Sm							3.64		
Eu							1.01		
Gd							3.46		
Tb							0.53		
Dy							3.40		
Ho							0.70		
Er							2.11		
Tm							0.31		
Yb							2.16		
Lu							0.33		
Hf							3.13		
Ta							0.44		
W							0.63		
Tl							0.24		
Pb							8.02		
Th							5.93		
Th*	9.80	7.80	10.2	6.90	11.6	6.00	6.50	7.10	8.40
U							1.31		
^{143}Nd/^{144}Nd									
^{87}Sr/^{86}Sr									
^{206}Pb/^{204}Pb									
^{207}Pb/^{204}Pb									
^{208}Pb/^{204}Pb									

IEGZN-	ME1562	ME1564	ME1565	ME1567	ME1568	ME1570	ME1571	ME1572	ME1573
Locality	53	54	54	54	55	56	57	58	58
Lat. [N]	37.606	37.606	37.606	37.606	37.609	37.610	37.612	37.595	37.595
Long. [E]	23.378	23.382	23.382	23.382	23.387	23.388	23.390	23.338	23.338
Elevation [m]	531.03	541.58	541.58	541.58	456.06	432.31	299.18	29.60	29.60
SiO_2	62.90	64.39	56.38	55.15	63.61	62.96	60.83	60.21	57.53
TiO_2	0.54	0.46	0.70	0.72	0.52	0.53	0.61	0.59	0.68
Al_2O_3	16.64	16.36	18.36	18.86	16.62	16.43	17.22	17.70	18.36
Fe_2O_3	4.96	4.35	7.32	7.64	4.82	4.95	5.87	5.91	6.97
MnO	0.11	0.11	0.15	0.15	0.11	0.11	0.12	0.13	0.14
MgO	2.32	1.94	3.21	3.42	2.15	2.21	2.88	2.91	3.64
CaO	5.67	5.20	7.47	7.74	5.52	5.57	6.23	6.72	7.43
Na_2O	3.31	3.52	3.59	3.25	3.39	3.48	3.77	3.37	3.24
K_2O	2.19	2.33	1.77	1.68	2.26	2.15	1.92	1.75	1.40
P_2O_5	0.11	0.10	0.14	0.14	0.13	0.11	0.15	0.15	0.15
LOI	1.08	1.09	0.76	1.09	0.73	1.36	0.23	0.41	0.32
Total	99.84	99.84	99.84	99.83	99.85	99.85	99.84	99.84	99.85
Li	23.0	25.8	16.9						
Sc	13.2	9.70	13.4						
V	79.3	78.9	135						
V*	84.5	81.5	152	156	77.2	81.5	113	110	130
Cr	23.3	15.4	4.4						
Cr*	26.9	17.4	6.70	17.4	20.2	26.7	22.1	59.3	27.9
Co	10.2	8.87	14.6						
Ni	6.91	6.35	2.90						
Ni*	4.30	7.40	4.20	2.10	7.20	5.90	8.90	30.3	14.7
Cu	8.84	8.60	5.05						
Zn	57.8	52.4	104						
Zn*	60.6	56.8	111	110	59.0	61.3	61.9	65.6	71.4
Ga	42.3	43.4	28.5						
Ga*	15.5	14.8	17.9	17.1	15.2	14.4	15.4	14.1	16.4
Rb	72.9	79.7	52.3						
Rb*	70.3	78.1	55.2	56.5	69.8	72.0	61.7	52.5	40.6
Sr	260	262	284						
Sr*	244	252	293	304	245	243	279	296	313
Y	21.1	16.1	24.6						
Y*	22.7	16.9	23.1	21.9	22.1	22.5	21.7	20.4	21.4
Zr	93.5	83.4	124						
Zr*	148	132	127	121	146	140	134	136	127
Nb	8.85	7.91	6.85						
Nb*	9.00	8.60	6.90	8.50	8.60	9.10	8.10	7.40	7.00

IEGZN-	ME1562	ME1564	ME1565	ME1567	ME1568	ME1570	ME1571	ME1572	ME1573
Mo	1.42	1.55	1.16						
Sn	1.75	1.49	1.02						
Cs	2.96	3.71	2.52						
Ba	445	492	360						
Ba*	447	455	355	350	430	391	398	381	319
La	26.1	25.0	20.3						
Ce	52.2	46.4	38.8						
Pr	5.60	4.76	4.58						
Nd	21.0	16.9	17.9						
Sm	4.10	3.13	3.95						
Eu	1.00	0.85	1.06						
Gd	3.81	2.83	3.87						
Tb	0.60	0.45	0.62						
Dy	3.78	2.81	4.04						
Ho	0.77	0.58	0.83						
Er	2.30	1.77	2.45						
Tm	0.34	0.28	0.37						
Yb	2.36	1.90	2.47						
Lu	0.35	0.30	0.38						
Hf	2.84	2.50	3.29						
Ta	0.64	0.63	0.44						
W	1.11	1.22	0.66						
Tl	0.38	0.43	0.35						
Pb	13.3	15.2	22.7						
Th	9.02	10.6	6.11						
Th*	7.30	9.60	5.00	5.50	9.30	8.00	8.20	6.20	5.90
U	2.06	2.58	1.40						
^{143}Nd/^{144}Nd	0.51238	0.51246	0.51250						
^{87}Sr/^{86}Sr	0.70738	0.70668	0.70737						
^{206}Pb/^{204}Pb	18.82	18.74	18.50						
^{207}Pb/^{204}Pb	15.69	15.68	15.67						
^{208}Pb/^{204}Pb	39.02	38.90	38.67						

IEGZN-	ME1574	ME1579	ME1580	ME1582	ME8415	ME1585	ME1592	ME1593
Locality	59	61	62	63	65	66	69	70
Lat. [N]	37.603	37.606	37.608	37.620	37.590	37.612	37.611	37.588
Long. [E]	23.332	23.347	23.353	23.324	23.356	23.401	23.374	23.391
Elevation [m]	77.40	465.03	541.40	192.78	134.17	234.98	584.64	94.91
SiO_2	58.68	60.34	61.51	54.40	61.69	61.07	58.19	58.80
TiO_2	0.58	0.60	0.61	0.76	0.55	0.67	0.64	0.68
Al_2O_3	17.54	17.39	17.34	17.69	17.40	17.37	17.96	17.89
Fe_2O_3	6.43	5.93	5.72	7.32	5.88	5.32	6.48	6.36
MnO	0.14	0.13	0.12	0.14	0.14	0.12	0.13	0.13
MgO	3.32	2.94	2.81	5.41	2.24	2.85	3.57	3.35
CaO	7.66	6.45	6.18	9.08	6.09	6.32	7.36	6.95
Na_2O	3.43	3.26	3.53	3.22	3.48	3.27	3.10	3.30
K_2O	1.65	1.83	1.87	1.34	1.78	1.94	1.72	1.72
P_2O_5	0.11	0.14	0.14	0.12	0.16	0.15	0.13	0.14
LOI	0.31	0.83	0.00	0.36	0.43	0.77	0.55	0.52
Total	99.85	99.84	99.84	99.84	99.85	99.84	99.84	99.84
Li		20.8				18.7		16.9
Sc		14.9				16.3		17.3
V		114				126		147
V*	136	101	111	180	92.5	122	125	136
Cr		20.2				20.6		12.3
Cr*	29.3	26.0	24.1	119	7.60	23.3	53.4	13.8
Co		13.3				13.1		16.7
Ni		9.21				12.9		9.04
Ni*	7.00	13.5	11.2	38.1	2.90	9.00	17.2	13.1
Cu		15.1				17.6		15.5
Zn		59.8				53.8		61.6
Zn*	73.8	65.7	63.4	60.3	72.0	57.0	68.0	65.4
Ga		40.4				44.8		42.2
Ga*	17.4	14.5	15.2	17.6	14.6	16.9	17.5	17.5
Rb		57.2				62.3		53.5
Rb*	53.5	56.9	58.5	43.8	49.1	60.2	46.7	52.6
Sr		301				303		313
Sr*	273	281	277	272	297	285	294	300
Y		19.2				19.7		18.6
Y*	21.4	21.0	19.6	21.4	22.0	21.0	20.6	19.4
Zr		98.7				90.7		97.3
Zr*	118	135	135	103	145	156	138	129
Nb		7.63				8.94		6.53
Nb*	7.50	9.90	8.80	7.10	8.00	8.20	9.00	7.70
Mo		1.21				1.18		1.05
Sn		2.21				2.63		1.59

IEGZN-	ME1574	ME1579	ME1580	ME1582	ME8415	ME1585	ME1592	ME1593
Cs		2.77				2.47		2.35
Ba		413				503		429
Ba*	346	386	415	267	413	461	370	396
La		22.3				24.6		19.9
Ce		43.7				52.2		40.3
Pr		4.86				5.42		4.49
Nd		18.6				20.5		17.5
Sm		3.71				4.05		3.57
Eu		1.00				1.07		1.00
Gd		3.47				3.71		3.37
Tb		0.54				0.58		0.53
Dy		3.41				3.60		3.30
Ho		0.70				0.73		0.68
Er		2.10				2.16		2.04
Tm		0.31				0.32		0.30
Yb		2.16				2.15		2.08
Lu		0.32				0.32		0.32
Hf		2.70				2.69		2.63
Ta		0.53				0.62		0.43
W		0.93				0.85		0.71
Tl		0.30				0.34		0.20
Pb		10.3				10.7		9.70
Th		7.60				8.07		6.51
Th*	6.80	7.00	7.30	4.60	5.40	7.00	6.10	4.70
U		1.86				1.79		1.54
^{143}Nd/ ^{144}Nd						0.51238		0.51253
^{87}Sr/ ^{86}Sr						0.70753		0.70669
^{206}Pb/ ^{204}Pb						18.87		18.90
^{207}Pb/ ^{204}Pb						15.70		15.69
^{208}Pb/ ^{204}Pb						39.06		39.03

Table 2. Detailed petrography description of selected thin sections.

ME15-12	enclave	basaltic andesite	50% plag up to 4.5mm, sub- to anhedral and partly sieve-textured; 20% biotite <3mm, subhedral and elongated; 15% amph <1mm, sub- to anhedral, strongly altered with secondary rims (px?); 3% subhedral Fe- Ti oxides <40μm; matrix of microfibrous plagioclase needles (<200μm); 5% cavities.
ME15-46	lava	dacite	25% plag up to 4.5mm, sub- to anhedral and partly sieve-textured; 15% amph <3.5mm, eu- to subhedral; 10% anhedral biotite <1.5mm; less than 5% subhedral Fe-Ti oxides up to 600μm; 3% anhedral pyroxene, cpx <800μm, opx <140μm; 2% subhedral olivine <200μm; 45% matrix of microfibrous plagioclase needles (<200μm); 2% cavities.
ME15-49	Enclave 1	basalt	35% plag <1.2mm, eu- to subhedral, partly sieve-textured; 25% sub- to anhedral amph <200μm; 10% biotite < 800μm; 5% Fe-Ti oxides <200μm; 15% sub- to anhedral px, cpx <800μm, opx <240μm; <5% subhedral olivine <250μm; 5% cavities.
ME15-49	Enclave 2	basalt	35% plag up to 4mm, sub- to anhedral, partly soluted and sieve-textured; 20% anhedral, strongly altered biotite <2.5mm; 15% strongly altered, anhedral amph <100μm; 10% anhedral Fe-Ti oxides <600μm; 5% subhedral px, cpx <400μm, opx <240μm; 1% subhedral olivine <320μm; 10% matrix of microfibrous plagioclase needles (<400μm); 5% cavities.
ME15-61	lava	dacite	20% plag up to 4mm, sub- to anhedral; 10% euhedral- to subhedral amph <3mm; 10% anhedral, elongated biotite <4mm; 5% anhedral Fe-Ti oxides <120μm; 1% anhedral opx <600μm; 45% matrix of microfibrous plagioclase needles (<600μm); 10% cavities.
ME15-61	Enclave 1		15% plag up to 800μm, sub- to anhedral, partly sieve-textured; 15% sub- to anhedral amph <400μm; 10% anhedral, elongated biotite <800μm; 3% anhedral Fe-Ti oxides <100μm; 1% subhedral olivine <400μm; 50% matrix of microfibrous plagioclase needles (<160μm); 6% cavities.
ME15-61	Enclave 2		10% plag up to 1.6mm, eu- to subhedral, partly sieve-textured; 15% subhedral amph <1.5mm; 15% anhedral, elongated biotite <2mm; 5% anhedral Fe-Ti oxides <400μm; 40% matrix of euhedral, elongated, fibrous plag; 15% cavities.

ME15-64	Lava	dacite	20% plag up to 2.4mm, eu- to subhedral; 10% subhedral amph <1.2mm; 10% anhedral biotite <2mm; 5% anhedral Fe-Ti oxides <800μm; 2% subhedral opx <400μm; <50% matrix of microfibrous plagioclase needles (<20μm); 5% cavities.
ME15-68	lava	dacite	30% plag up to 4mm, sub- to anhedral, partly sieve-textured; 15% sub- to anhedral amph <320μm; 10% anhedral, partly strongly altered biotite <800μm; 5% anhedral Fe-Ti oxides <400μm; 5% anhedral opx <1.2mm; 35% matrix of microfibrous plagioclase needles (<80μm).
ME15-68	enclave		30% plag up to 1.6mm, subhedral, partly sieve-textured; 15% sub- to anhedral amph, <600μm; 10% subhedral, elongated biotite <1.6mm; <2% anhedral opx <600μm; <1% anhedral Fe-Ti oxides <400μm; >40% cavities.
ME15-72	lava	andesite	25% plag up to 1.4mm, subhedral, partly sieve-textured; 5% anhedral biotite <4mm; 5% subhedral Fe-Ti oxides <1.2mm, often shaped like amph; 2% anhedral opx <400μm; 1% anhedral olivine <120μm; <1% euhedral amph <300μm; 10% cavities.
ME15-85	lava	andesite	30% plag up to 4.3mm, subhedral, partly sieve-textured; 6% sub- to anhedral px <400μm, opx often grown together with cpx; 5% amph <1.2mm, strongly altered, sieve-textured or crisscrossed by px and Fe-Ti oxides; 5% sub- to anhedral, strongly altered biotite <1.2μm; 5% anhedral Fe-Ti oxides <400μm; 4% olivine <1mm; 35% matrix of microfibrous plagioclase needles (<60μm); 10% cavities.
ME15-85	enclave		20% plag up to 800μm, subhedral, partly sieve-textured; 10% anhedral px, cpx <400μm, opx <320μm; 10% subhedral, elongated olivine <400μm; 8% anhedral Fe-Ti oxides <160μm; 5% subhedral olivine <300μm; 2% amph <600μm, strongly altered, sieve-textured or crisscrossed by px and Fe-Ti oxides; 35% matrix of microfibrous plagioclase needles (<200μm); 5% cavities.
ME15-89	lava	andesite	20% plag up to 4.3mm, subhedral, partly sieve-textured; 15% sub- to anhedral biotite <4mm; 10% eu- to subhedral amph <2mm; 10% anhedral px, cpx <1.6mm, opx <400μm; 5% anhedral Fe-Ti oxides <800μm; 5% subhedral olivine <240μm; 30% matrix of microfibrous plagioclase needles (<30μm).

Table 3. Parameters used in the EC-RAFC modelling.

	Sr	**Nd**	**Pb**	**Th**
Magma conc.	230	10	8	2.5
Bulk D	0.54	0.33	0.12	0.01
Assimilant conc.	400	26	30	6
Bulk D	0.6	0.35	0.25	0.01
	$^{87}Sr/^{86}Sr$	**$^{143}Nd/^{144}Nd$**	**$^{206}Pb/^{204}Pb$**	
Magma isotope ratio	0.7055	0.51265	18.8	
Assimilant isotope ratio	0.7115	0.5121	19.0	